Paleoceanography and Paleoclimatology

RESEARCH ARTICLE
10.1029/2018PA003364

Key Points:
- Independent of the shoaling stage, the Central American Seaway altered the ocean mean state and deep water properties globally
- The seaway provided a shortcut for Pacific water, transporting heat and salt to the South Atlantic
- The seaway suppressed Antarctic Bottom Water northward extent, allowing North Atlantic Deep Water to deepen and slightly strengthen

Supporting Information:
- Supporting Information S1

Correspondence to:
L. T. Sentman,
lori.sentman@noaa.gov

Citation:
Sentman, L. T., Dunne, J. P., Stouffer, R. J., Krasting, J. P., Toggweiler, J. R., & Broccoli, A. J. (2018). The mechanistic role of the Central American Seaway in a GFDL Earth System Model. Part 1: Impacts on global ocean mean state and circulation. *Paleoceanography and Paleoclimatology*, *33*, 840–859. https://doi.org/10.1029/2018PA003364

Received 14 MAR 2018
Accepted 26 JUN 2018
Accepted article online 3 JUL 2018
Published online 27 JUL 2018

The Mechanistic Role of the Central American Seaway in a GFDL Earth System Model. Part 1: Impacts on Global Ocean Mean State and Circulation

Lori T. Sentman[1], John P. Dunne[1], Ronald J. Stouffer[1], John P. Krasting[1], J. R. Toggweiler[1], and Anthony J. Broccoli[2]

[1]National Oceanic and Atmospheric Administration/Geophysical Fluid Dynamics Laboratory, Princeton, NJ, USA, [2]Department of Environmental Sciences and Institute for Earth, Ocean, and Atmospheric Sciences, Rutgers, State University of New Jersey, New Brunswick, NJ, USA

Abstract To explore the mechanisms involved in the global ocean circulation response to the shoaling and closure of the Central American Seaway (CAS), we performed a suite of sensitivity experiments using the Geophysical Fluid Dynamics Laboratory Earth System Model (ESM), GFDL-ESM2G, varying only the seaway widths and sill depths. Changes in large-scale transport, global ocean mean state, and deep ocean circulation in all simulations are driven by the direct impacts of the seaway on global mass, heat, and salt transports. Net mass transport through the seaway into the Caribbean is 20.5–23.1 Sv with a deep CAS but only 14.1 Sv for the wide, shallow CAS. Seaway transport originates from the Antarctic Circumpolar Current in the Pacific and rejoins it in the South Atlantic, reducing the Indonesian Throughflow and transporting heat and salt southward into the South Atlantic, in contrast to present-day and previous CAS simulations. The increased southward salt transport increases the large-scale upper ocean density, and the freshening and warming from the changing ocean transports decreases the intermediate and deep water density. The ocean circulation pathway with a CAS traps heat in the Southern Hemisphere oceans and reduces the northern extent of Antarctic Bottom Water penetration in the Atlantic, strengthening and deepening Atlantic meridional overturning, in contrast to previous studies. In all simulations, the seaway has a profound effect on the global ocean mean state and alters deep water mass properties and circulation in the Atlantic, Indian, and Pacific basins, with implications for changing deep water circulation as a possible driver for changes in long-term climate.

1. Introduction

Improved understanding of the underlying mechanisms driving changes in global ocean circulation, and thereby oceanic heat uptake, and their effect on climate during past warm climates is instrumental for improved decadal predictions and future climate projections. The gradual shoaling of the Central American Seaway (CAS) during the Pliocene (5.3–2.6 Ma) restricted an important circulation pathway of mass, heat, and salt exchange between the Pacific and Atlantic Oceans. Mixed-layer δ^{18}O planktonic foraminifera (*Globigerinoides sacculifer*) records (Keigwin, 1982) and Cd/Ca measurements (Maier-Reimer et al., 1990) for the mid-Miocene (~15 Ma) suggest that prior to 4 Ma sea surface salinity (SSS) in the eastern equatorial Pacific (EEP) and Caribbean were similar. Divergence in mixed-layer δ^{18}O records between Pacific (site 503) and Atlantic (site 502) Deep Sea Drilling Project sites indicates a 0.5–1.0‰ increase in Atlantic SSS after 4.2 Ma consistent with the modern-day Pacific-Atlantic SSS contrast (Keigwin, 1982). Furthermore, ~4.4 Ma diverging planktonic foraminifera δ^{18}O records from the Caribbean and EEP indicate a buildup of the modern Pacific-Caribbean salinity contrast (Figure S1 in the supporting information; Haug et al., 2001). These records are also consistent with increasing foraminiferal Mg/Ca ratios ~4.4 Ma indicating rising temperatures in the Caribbean (Groeneveld et al., 2008). The consensus of proxy data for the Pliocene and idealized CAS climate models (Molnar, 2008, and references therein) indicate a significant change to the salinity and temperature water mass characteristics between the Pacific and Caribbean, hypothesized to be from the gradual shoaling and closure of the CAS. However, there remains uncertainty in how the changing water mass properties from the seaway shoaling affect deep ocean circulation and what mechanisms (e.g., reduced Antarctic Bottom Water [AABW] extent allowing North Atlantic Deep Water [NADW] to penetrate deeper) drive changes in the tropics to changes in high latitude deep water.

The δ^{13}C records from benthic foraminifera, *Cibicidoides*, (Woodruff & Savin, 1989) suggest that NADW production increased after 10–12 Ma, significantly before the CAS shoaling. In contrast, higher benthic δ^{13}C values and better carbonate preservation in the Caribbean at Ocean Drilling Program (ODP) Site 999 (12°44′N, 78°44′W, Colombian basin, water depth of 2,828 m) between 5 and 2 Ma indicate stronger ventilation attributed to intensification of NADW in association with the gradual shoaling and closure of the CAS (Haug & Tiedemann, 1998). Recently, Bell et al. (2015) analyzed δ^{13}C and δ^{18}O from ODP sites in the Atlantic, including the South Atlantic—a key area for the southern extent of NADW—and concluded that deep water formation was as strong and frequently stronger during the early Pliocene (~4.7 Ma) compared to present day (Figure S2 in the supporting information). Furthermore, climate models found that the CAS transported relatively fresh and cool Pacific water into the Atlantic, decreasing SSS in the Caribbean and Atlantic Ocean, and either shutdown (Maier-Reimer et al., 1990; Mikolajewicz et al., 1993; Mikolajewicz & Crowley, 1997; Murdock et al., 1997) or weakened (Butzin et al., 2011; Klocker et al., 2005; Lunt et al., 2008; Nisancioglu et al., 2003; Schneider & Schmittner, 2006; Steph et al., 2006, 2010; Yang et al., 2013; Zhang et al., 2012) the Atlantic meridional overturning circulation (AMOC). Diversity in the AMOC responses among these models has been attributed to varying ocean model parameterizations, such as ocean diffusivity (Schneider & Schmittner, 2006), leading to considerable uncertainty in the magnitude of changes in AMOC and the spatial extent of changes in global deep water circulation with a seaway in both paleoclimate proxy data and climate models. Furthermore, divergence in interpretations of available proxy data may represent different stages in the evolution of the CAS. Improved understanding and model representation of past deep water circulation response to freshwater fluxes is valuable for decadal predictions and future climate projections.

Models of various complexity show that the AMOC is sensitive to changes in extratropical salinity fluxes (Bryan, 1986; Manabe & Stouffer, 1988; Mikolajewicz & Maier-Reimer, 1994; Rahmstorf, 1995; Schiller et al., 1997; Stommel, 1961; Yin & Stouffer, 2007), and changes in AMOC impact global climate through changes in interhemispheric heat flux (Broecker, 1998; Stocker, 1998) and may contribute to abrupt climate transitions (Manabe & Stouffer, 1988). Recently, Delworth and Zeng (2016) demonstrated that the positive phase of the North Atlantic Oscillation strengthens the AMOC and increases horizontal density gradients and deep water formation. However, the rate and magnitude of changes in AMOC in response to changes in future climate is very uncertain (Kirtman et al., 2013). The detection and attribution of the underlying mechanisms driving changes in global ocean circulation and their effect on climate from the gradual shoaling and closure of the CAS provides valuable insight on how these mechanisms may respond to future changes in climate.

We perform idealized open/closed seaway sensitivity simulations with a Geophysical Fluid Dynamics Laboratory (GFDL) fully coupled carbon-climate/Earth System Model, GFDL-ESM2G, to better understand and quantify the mechanistic role of the various stages of CAS shoaling on ocean mean state and deep water circulation. We simulate the evolution of the CAS via different model bathymetry representations from early to late CAS shoaling stages. To our knowledge, these are the first CAS sensitivity simulations that use an ESM with high enough spatial resolution in the ocean component capable of simulating a very narrow, single-point channel without significant regional alteration of topography or land-sea mask.

2. Experimental Design

2.1. Model Description

GFDL-ESM2G (Dunne et al., 2012, 2013; T1 in the supporting information and references therein including Delworth et al., 1998; Fox-Kemper et al., 2011; Hallberg, 2003; Milly et al., 2014; Simmons et al., 2004; Thompson et al., 2003) participated in the most recent Coupled Model Intercomparison Project version 5 (CMIP5; Taylor et al., 2012). To our knowledge, the ocean component in previous climate models (Butzin et al., 2011; Klocker et al., 2005; Lunt et al., 2008; Nisancioglu et al., 2003; Schneider & Schmittner, 2006; Steph et al., 2006, 2010; Yang et al., 2013; Zhang et al., 2012) had relatively coarse resolution compared to GFDL-ESM2G (1° horizontal increasing to 1/3° meridionally at the equator and 63 vertical levels) and may not have resolved important aspects of the circulation that depend critically on the parameterized subgrid-scale processes, such as deep water formation processes, undercurrent, and equatorial tropical instability waves, that are represented in GFDL-ESM2G. GFDL-ESM2G provides a better representation of boundary currents than relatively coarser ocean models and reasonable resolution across varying density water structures

Table 1
GFDL-ESM2G Experiment Design and Ocean Mean State

Simulation	Seaway depth (m)	Seaway width (km)	Meridional[a] OHT[b] at 30°N (PW)	Meridional[a] OHT[b] at 30°S (PW)	Meridional[a] salt transport[b] at 30°N (10^6 kg/s)	Meridional[a] salt transport[b] at 30°S (10^6 kg/s)	Global SST[b] (°C)	Global SSS[b] (psu)	Global upper 100-m ocean density[b] (kg/m^3)
CLOSED	0	0	1.68	−0.52	−0.09	−0.06	17.89	34.13	1024.87
NARROW	2000	~100	1.56	−0.56	−0.20	−.0.21	18.21	34.56	1025.12
WIDESHALLOW	200	~2,000	1.60	−0.61	−0.51	−0.25	18.43	34.53	1025.05
WIDE	2000	~2,000	1.56	−0.63	−0.77	−1.64	18.45	34.61	1025.09

Note. GFDL-ESM2G = Geophysical Fluid Dynamics Laboratory Earth System Model Version 2G; OHT = ocean heat transport; SSS = sea surface salinity; SST = sea surface temperature.
[a]Northward positive, vertical depth integrated. [b]One hundred-year annual average.

(e.g., Southern Ocean, bottom waters to low latitudes, and marginal seas; Dunne et al., 2012). This model was chosen for its good representation of the present-day climate mean state, its ability to preserve water mass structure using a diapycnal mixing scheme (Hallberg, 2000), and its horizontal grid discretization capability of simulating realistic flows through very narrow channels (Dunne et al., 2012), an important characteristic in simulating the evolution of the CAS. The background diapycnal diffusivity (K_d) described in Harrison and Hallberg (2008) is 2×10^{-6} m^2/s at the equator and increases to 2×10^{-5} m^2/s at 30°N, representing realistic spatial dependence of global ocean vertical mixing, a model-dependent parameterization that ocean overturning is particularly sensitive to in CAS studies (Schneider & Schmittner, 2006).

GFDL-ESM2G NADW formation and circulation is characterized by realistic southward NADW flow and agrees well with observationally based estimates (Ganachaud & Wunsch, 2003; Talley, 2003) for the streamfunction depth scale (Dunne et al., 2012). There is a high salinity and warm bias from strong deep Pacific ventilation from the south (16 Sv; 1 Sv = 1×10^6 m^3/s) and the maximum overturning (22 Sv at 24°N) is higher and shallower than observationally based estimates (17.2–19.8 Sv; Talley, 2003; Ganachaud & Wunsch, 2003). In the Atlantic, AABW upwells to a depth of ~3 km before flowing southward out of the basin. The ventilation/flushing timescales, as determined by the ideal age tracer in the model, compares well with radiocarbon-based estimates (Krasting et al., 2016). Globally, GFDL-ESM2G agrees well with observational estimates of ocean heat transport (OHT; Dunne et al., 2012). Atlantic meridional OHT at 26.5°N in the model (1.14 PW) is within the range of estimates from the Rapid Climate Change program, RAPID (1.33 ± 0.40 PW; Johns et al., 2011). Dunne et al. (2012) provide comprehensive model documentation and finds that the GFDL-ESM2G preindustrial (year 1860) quasi-equilibrium simulation produces sufficient fidelity to allow meaningful perturbation studies and the model's framework (e.g., spatial resolution, vertical diffusion, and water mass characteristics) addresses deficiencies from previous CAS studies.

2.2. Idealized Experiments

There is considerable uncertainty in the paleoclimate record regarding the exact details of the paleogeography (Figure S3 in the supporting information; Coates & Obando, 1996; Kirby & MacFadden, 2005; Whitmore & Stewart, 1965), the timing of the CAS shoaling and closure (de Boer et al., 1995; Coates et al., 2004; Collins et al., 1995; Corrigan et al., 1990; Duque-Caro, 1990; Lonsdale & Klitgord, 1978; Marshall, 1985; Molnar, 2008; Montes, Bayona, et al., 2012, Montes, Cardona, et al., 2012; Osborne et al., 2014; Sepulchre et al., 2014; Sykes et al., 1982; Webb, 1985; Webb & Rancy, 1996), and its effect on deep water circulation during the Pliocene (Bell et al., 2015; Billups et al., 1998; Burton et al., 1997; Driscoll & Haug, 1998; Frenz et al., 2006; Haug & Tiedemann, 1998; Haug et al., 2001; Ishman, 1996; Steph et al., 2010; Osborne et al., 2014; Woodruff & Savin, 1989; Wold, 1994). Rather than simulating the realistic comprehensive suite of changes to the Earth system associated with the climate of the Pliocene, we instead examine the mechanistic role of changing topography associated with the various stages of CAS closure on global ocean circulation through four open/closed CAS sensitivity experiments (Table 1) with all other model forcing (e.g., continental configuration and climate forcing, such as well-mixed greenhouse gases, aerosols, solar forcing, and orbital parameters) remaining constant. This experimental design is important for attribution studies since it isolates the impact of the evolution of the CAS on ocean mean state and deep water circulation. The "CLOSED" seaway simulation (Figure 1a) is identical to the CMIP5 GFDL-ESM2G preindustrial 1860 control experiment (Dunne et al., 2012, 2013). Three open CAS experiments ("NARROW," "WIDESHALLOW," and "WIDE") were

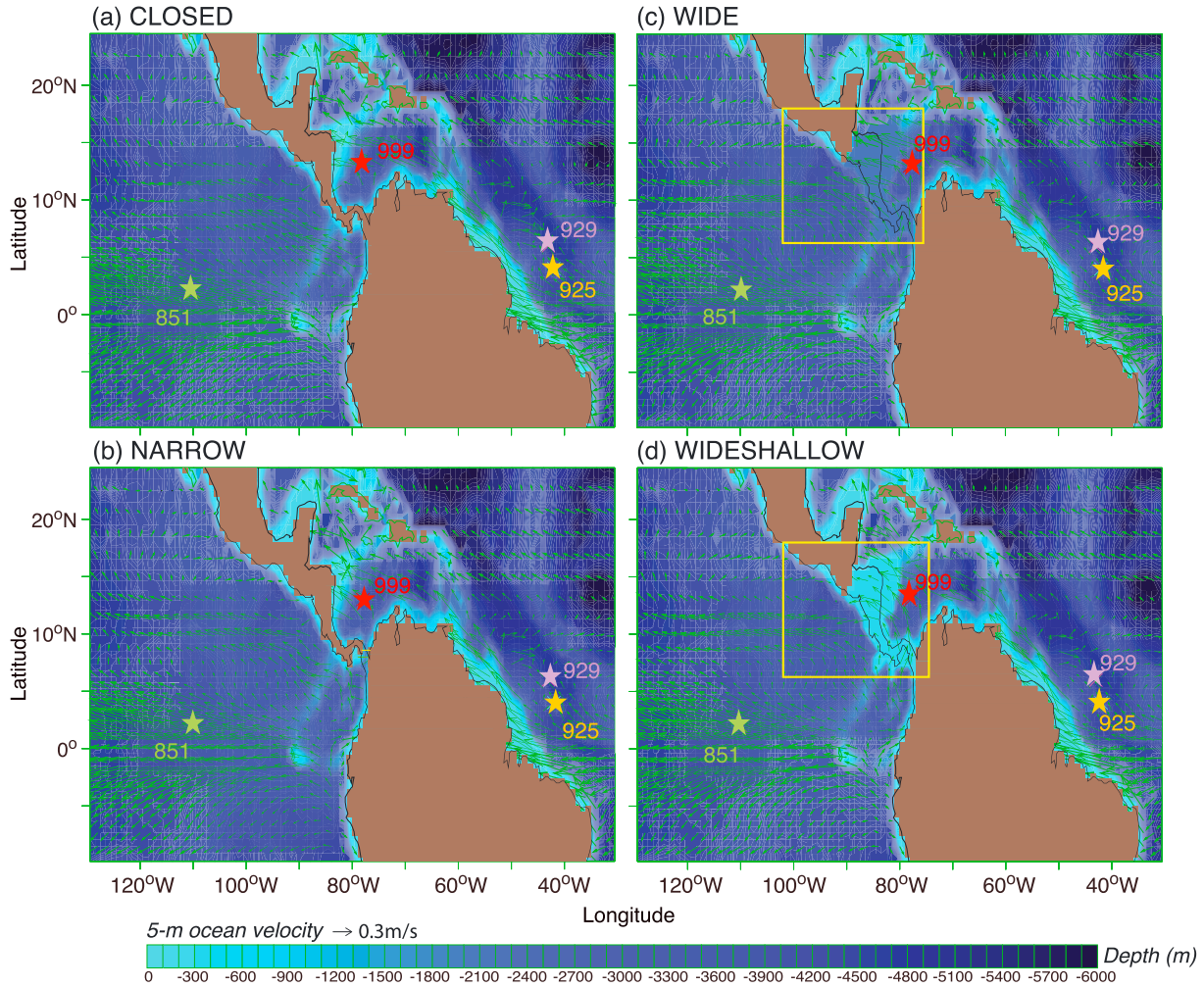

Figure 1. GFDL-ESM2G bathymetry (m; shaded) for (a) CLOSED, (b) NARROW, (c) WIDE, and (d) WIDESHALLOW and 5-m ocean velocity (m/s; green vectors). Xs show locations of Ocean Drilling Program sites 999 (red), 851 (green), 929 (purple) and 925 (yellow) referenced in Figure S1 in the supporting information. The yellow boxes (18°–8°N; 100°–77°W; [c] and [d]) and transect (77.5°W; 8.2°N; [b]) are used for WIDE/WIDESHALLOW and NARROW transport calculations, respectively. See Table 1 for the CAS widths and depths. GFDL-ESM2G = Geophysical Fluid Dynamics Laboratory Earth System Model Version 2G.

initialized from and are identical to CLOSED except for varying seaway widths and sill depths representing the various stages of seaway shoaling (Table 1).

A ~100-km-wide (e.g., one ocean model grid cell) and 2,000-m-deep seaway was introduced meridionally near the border of Central America (CA) and South America based on the peninsula model paleogeographic reconstruction of CA for the mid-Miocene (Figure S3b in the supporting information; Whitmore and Stewart, 1965) in the NARROW experiment (Figure 1b). This experiment is representative of the later stages of seaway closure. The WIDE experiment represents the earlier stages of seaway closure with a ~2,000-km-wide and 2,000-m-deep seaway (Figure 1c), similar to previous climate model studies (Figure S3c in the supporting information, Haug & Keigwin, 2004). To represent the archipelago paleogeographic reconstruction of CA separated by shallow straits for the mid-Miocene (Figure S3a in the supporting information; Coates & Obando, 1996) and simulate the seaway sill shoaling, the WIDESHALLOW experiment (Figure 1d) sill depth was raised to 200 m with the same width as WIDE. However, the timing and structure of the paleogeography of southern CA before the Isthmus of Panama remains unclear (Kirby & MacFadden, 2005). Therefore, this experimental design allows for a sensitivity study (via CAS snapshots) of the role of the gradual seaway shoaling (WIDE/early stages, NARROW/peninsula model, and WIDESHALLOW/archipelago model) on global ocean mean state and circulation and provides a framework for reconciliation with available proxy data and comparison with previous models.

Each experiment was initialized from present-day observed World Ocean Atlas 2005 temperature (Locarnini et al., 2006) and salinity (Antonov et al., 2006) and integrated for at least 1,400 model years toward a "quasi-equilibrium" 1860 state defined by the same qualitative metrics defined for the CMIP5 GFDL ESM "piCTRL" simulations (Dunne et al., 2012). This integration period is longer than the global ocean flushing timescale (~1,000 years) and is sufficient to allow for the deep ocean to adjust to the seaway perturbation (Figure S4 in the supporting information and Figure 2e). As quasi-equilibrium was established, we chose the final 100 years of the 1,400-year spin-up integrations (model years 1301–1400) as our analysis period, except for the AMOC calculations (Figure 2e) where we used the final 500-year period (model years 1001–1500) of the spin-up to capture the long-term climate variability. To better quantify and understand the role of the seaway on the global ocean mean state and circulation, we focus our analysis on the open seaways (e.g., NARROW, WIDE, and WIDESHALLOW) minus the CLOSED seaway or our control experiment.

3. Results

3.1. Seaway Impacts on Global Ocean Circulation

The presence of a CAS, regardless of whether it is 200 or 2,000 m deep or 100 or 2,000 km wide, affects both the local CA and global ocean circulation throughout the water column in our simulations, with a major alteration being a warm, southward flowing current into the South Atlantic (Figure 3). As discussed earlier, climate models support the hypothesis that the CAS permits relatively fresh and cool Pacific water to flow into the North Atlantic, affecting buoyancy by adding freshwater to the North Atlantic and weakening the AMOC. With an open CAS, our results indicate northward flowing Antarctic Circumpolar Current (ACC) water in the South Pacific basin mainly joins and intensifies the North Equatorial Countercurrent through the CAS (Figure S5 in the supporting information) and into the South Atlantic (Figures 3b–3d and Figure S5 in the supporting information)—reducing present-day Indonesian Throughflow (ITF) transport (Figure 4)—driven by sea surface height (SSH) anomalies between the Pacific and Atlantic (Figure S6 in the supporting information). With an open CAS, the SSH anomaly difference between these two basins is reduced although a small difference is retained to support the Pacific to Atlantic net mass transport from factors such as friction and changes in deep water formation. For all open CAS configurations, incoming Pacific water through the CAS flows southward as a warm surface current into the South Atlantic (Figure S5 in the supporting information), rather than the North Atlantic as found with climate models, and strengthens the ACC between 35°S and 40°S and weakens the return flow represented by a slight northward shift of the ACC (Figures 3b–3d). That is, the CAS closure blocked this circulation pathway and the water was rerouted through the ITF. In addition, WIDE and WIDESHALLOW permit the South Equatorial Current to transport water through the open CAS into the Pacific through the central (WIDE and WIDESHALLOW) and northern (WIDE) portions of these seaways near the surface (Figures 4c and 4d). NADW penetrates into the Pacific for the deep sill seaways, NARROW and WIDE (Figures 5a, 5b, 6b, and 6c), and this interbasin, deep water exchange has implications for global changes in deep water circulation.

3.2. Seaway Impacts on Interbasin and Intrabasin Transport

The net horizontal mass transport shows the interbasin water mass exchange between the Pacific and Atlantic in the CAS region (Figure 5a). There is 20.5-Sv net horizontal mass transport through the NARROW seaway meridionally from the Pacific to the Atlantic through most of the seaway depth (Figure 5a). The net horizontal mass transport is 23.1 and 14.1 Sv for WIDE and WIDESHALLOW, respectively; 9 Sv more transport for the relatively deeper of the two wide seaways (Figure 5a). There is bidirectional horizontal mass transport at each vertical level through WIDE and WIDESHALLOW (Figure 5b; section 3.1; Figure S5 in the supporting information)—which is not present in NARROW since it is a single grid point channel (not included in Figure 5b)—resulting in similar net mass transport for the 2,000-m-deep NARROW and WIDE seaways (Figure 5a) despite relatively large differences (~1,900 km) in their width (Table 1).

The upper 10-m ocean transports only a very small amount of mass through the CAS; 1.7%, 4.0%, and 2.3% of the net horizontal mass transport for NARROW, WIDESHALLOW, and WIDE, respectively (Figure 5a). The maximum interbasin transport through the CAS is in the upper (10–571 m) ocean for all open CAS configurations with WIDE transporting the most mass, (15.8 Sv) at this level, and NARROW transporting the most mass (8.9 Sv) below this level at 571–1,469 m (Figure 5a). The reversal of interbasin transport in NARROW and

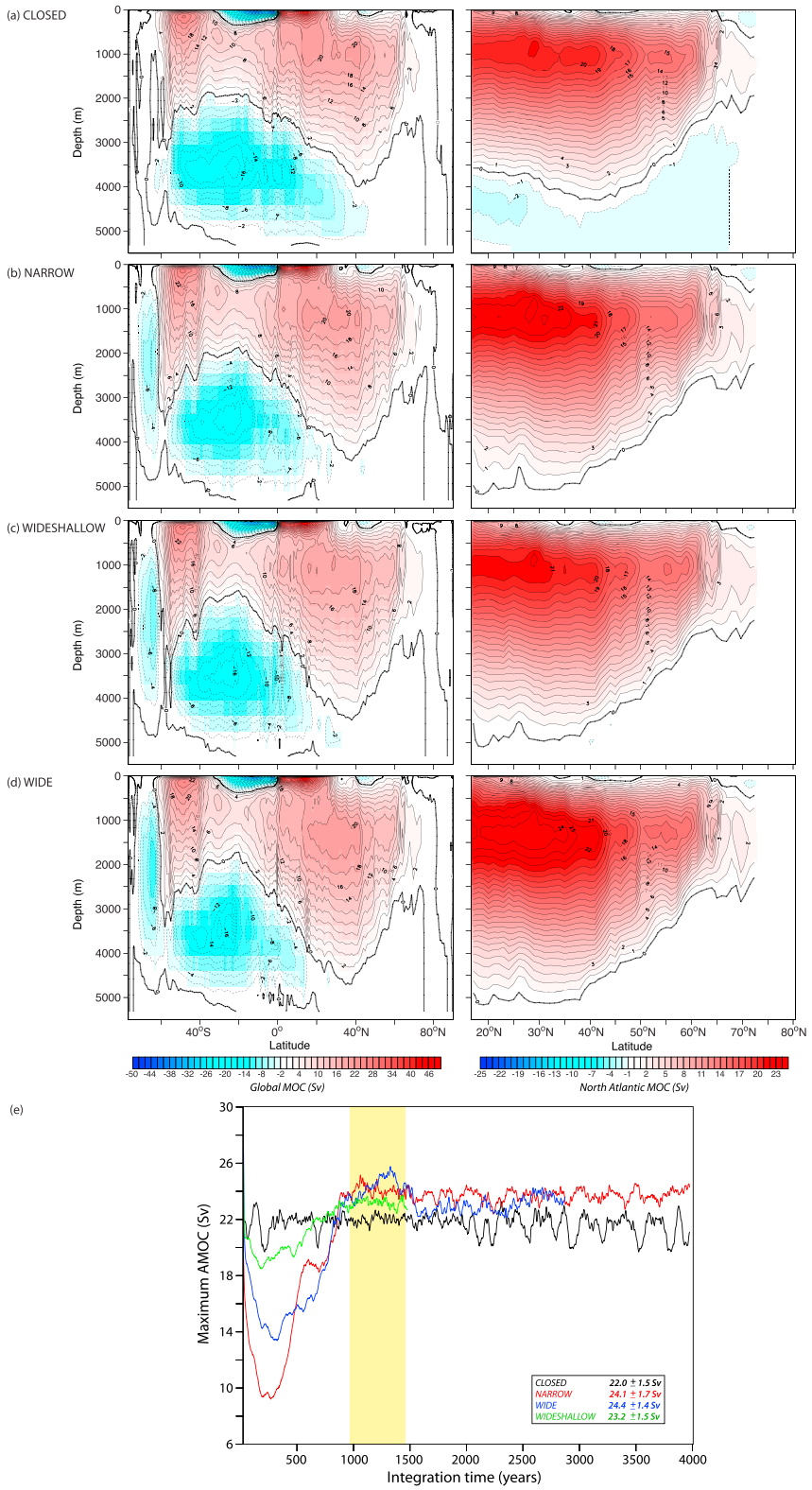

Figure 2. GFDL-ESM2G 100-year annual average global (left) and North Atlantic (right) meridional overturning streamfunction (1 Sv = 10^6 m^3/s) for (a) CLOSED, (b) NARROW, (c) WIDESHALLOW, and (d) WIDE. Positive (negative) values in red (blue) indicate clockwise (counterclockwise) circulation. (e) Maximum Atlantic Meridional Overturning Circulation (AMOC; Sv) time series in density space from 20°N to 80°N for the CLOSED (black), NARROW (red), WIDESHALLOW (green), and WIDE (blue) seaway experiments for model integration years 1–4000. The yellow shading (e) indicates the 500-year period (1001–1500) used in the maximum AMOC computation. Fifty-year boxcar smoothing is applied. GFDL-ESM2G = Geophysical Fluid Dynamics Laboratory Earth System Model Version 2G.

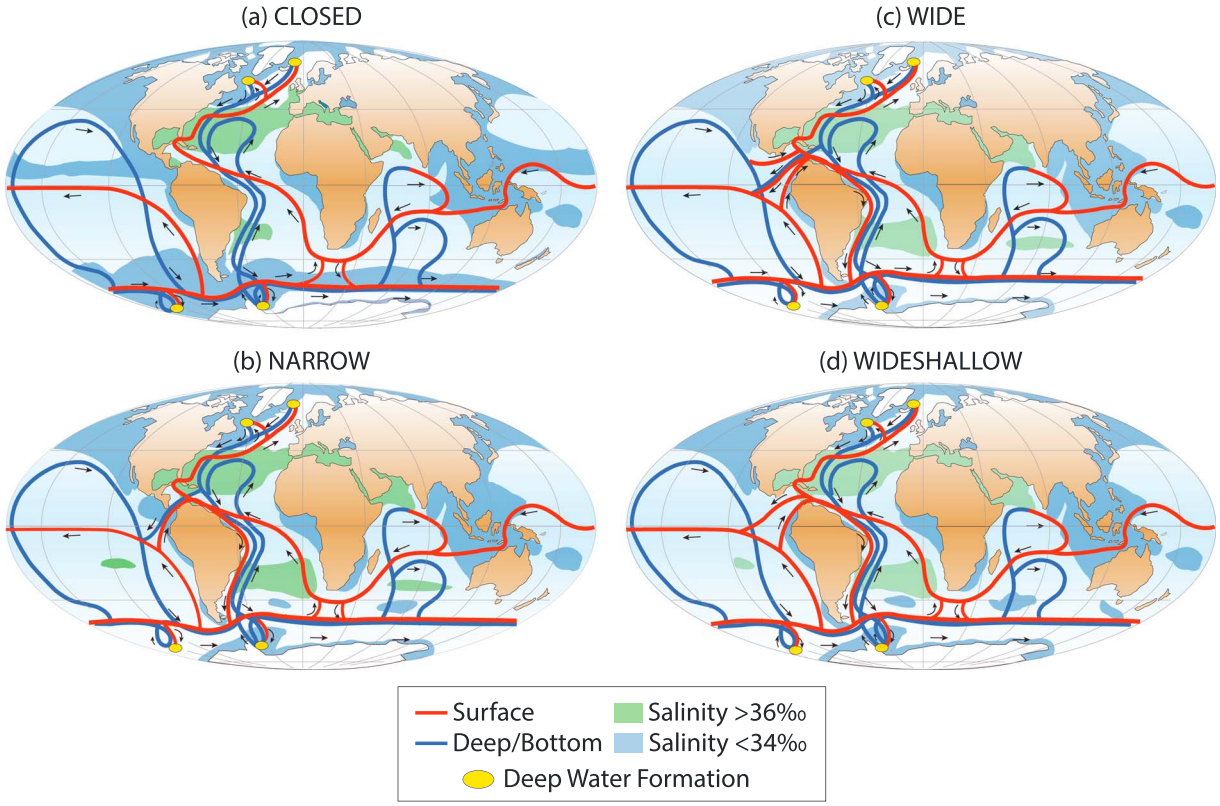

Figure 3. GFDL-ESM2G simplified global ocean circulation modified from Rahmstorf (2002) for (a) CLOSED, (b) NARROW, (c) WIDE, and (d) WIDESHALLOW derived from vertically integrated velocity vectors at various levels. Red (blue) lines indicate surface (deep/bottom) waters. Yellow ovals indicate deep water formation regions. Shading represents regions with salinity >36 psu (green) and <34 psu (blue) modified from Rahmstorf (2002) to reflect GFDL-ESM2G salinity. GFDL-ESM2G = Geophysical Fluid Dynamics Laboratory Earth System Model Version 2G.

WIDE where NADW penetrates into the Pacific through the CAS is evident below 1,469 m, with 12.8% of NARROW net mass transport below this depth (Figure 5a).

The box chosen for the mass transport computation in WIDESHALLOW (Figure 1d) includes ocean areas extending beyond the location of the CAS with depths greater than the 200 m sill depth, so that the bidirectional mass transport characterizes both the interbasin and intrabasin exchange with WIDESHALLOW (Figure 5b). The bidirectional mass transport in the bottom two levels (571–5,499 m), below the WIDESHALLOW sill depth, indicates that ~2 Sv is intrabasin mass exchange (Figure 5b) within the calculation box (Figure 1d). Similar to net mass transport, most of the interbasin exchange is at 10–571 m and the Pacific to Atlantic transport is ~2 times greater than the Atlantic to Pacific transport with WIDE and WIDESHALLOW (Figure 5b). Vertically integrated mass transport through all seaways is from the Pacific to Atlantic and suggests that interbasin heat and salt transports are fundamentally altered as the CAS shoals and narrows.

We quantify the alteration in global ocean circulation pathways with a seaway described in section 3.1 using the vertically integrated interbasin exchanges of mass, heat, and salt (Figure 4). The present-day ocean configuration in GFDL-ESM2G transports 22.3 Sv northward from the ACC in the South Pacific, with the majority (21.1 Sv) transported from the Pacific into the Indian Ocean via the ITF and 0.88 Sv transported northward into the Arctic Ocean via the Bering Strait (Figure 4a). The presence of a CAS in GFDL-ESM2G draws the northward extension of the ACC water in the South Pacific through the CAS and into the Caribbean, driven by the SSH anomalies across the CAS region between the Pacific and Atlantic basins (Figure S6 in the supporting information), rather than through the ITF. In CLOSED, the SSH anomaly difference between the Pacific and Atlantic is ~0.8–1 m in CLOSED and decreases to ~0.4–0.6 m in NARROW (Figure S6 in the supporting information). Mass transport through the open CAS decreases ITF mass transport by 82% for the WIDE and NARROW deep sills and 59% for the WIDESHALLOW relatively shallow sill (Figure 4a). The circulation through the open CAS also decreases mass transport into the Arctic Ocean via the Bering Strait and thereby southward mass transport

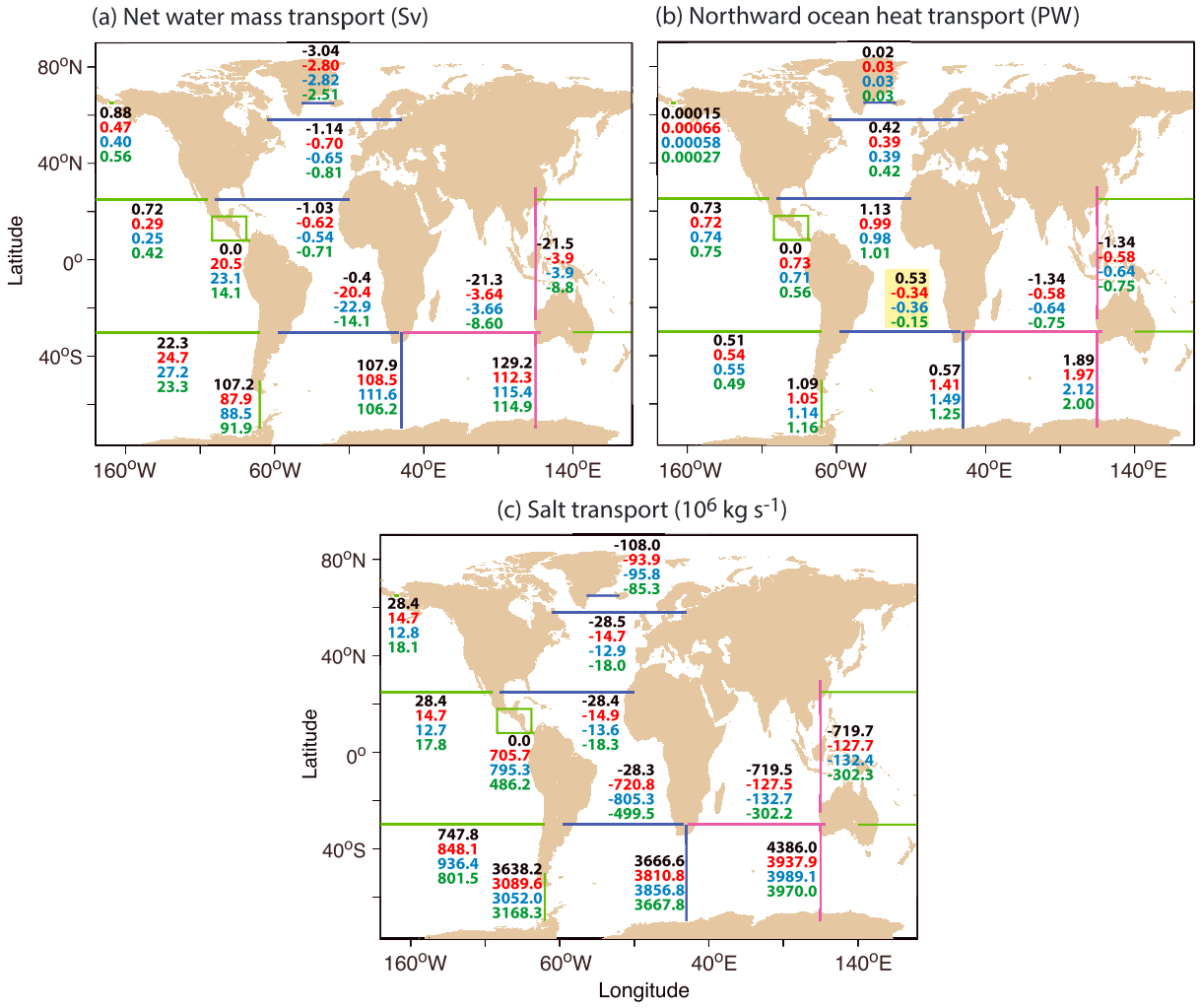

Figure 4. GFDL-ESM2G 100-year annual average (a) net water mass (Sv; 10^6 m^3/s), (b) ocean heat (PW), and (c) salt (10^6 kg/s) transport calculated for CLOSED (black), NARROW (red), WIDE (blue), and WIDESHALLOW (green) for 13 transects in the Pacific (green), Atlantic (blue), and Indian (magenta) Oceans. Total transport integrated from 0 to 5,499 m with northward/eastward (southward/westward) positive (negative). Bering Strait (green) at 65°N; North Pacific Ocean (green) at 25°N; South Pacific Ocean (green) at 30°S; CAS NARROW (green) at 77.5°W and 8.2°N; CAS WIDE and WIDESHALLOW (green) at 18°–8°N and 100°–77°W; Drake Passage (green) at 70°W; Denmark Strait (blue) at 65°N; GIN Seas/Denmark Strait/Labrador Sea (blue) at 58°N; North Atlantic (blue) at 25°N; South Atlantic (blue) at 30°S; Africa to Antarctica (blue) at 25°E; South Indian Ocean (magenta) at 30°S; Indonesian Throughflow (magenta) at 115°E; Australia to Antarctica (magenta) at 115°E. Yellow shading (b) indicates transport direction reversal. GFDL-ESM2G = Geophysical Fluid Dynamics Laboratory Earth System Model Version 2G; GIN = Greenland, Iceland, and Norwegian.

into the North Atlantic from the Arctic by ~36 to 55% (Figure 4a). Additionally, Pacific water flowing through the open CAS increases southward mass transport in the South Atlantic by a similar magnitude as the net CAS water mass transport (Figure 4a). This suggests that the ACC water rerouted through the CAS—instead of through Drake Passage—has a propensity for rejoining the ACC from which it originated, as opposed to following an alternative pathway, such as into the North Atlantic, North Pacific, or Indian Oceans.

The changing water mass transports driven by the SSH anomalies across the CAS region and between the Pacific and Atlantic (Figure S6 in the supporting information) with the addition of a CAS are also accompanied by changes in heat transports (Figure 4b). The northward flowing ACC water along South America in the South Pacific is only slightly (~4% to 8%) warmer with a seaway than present day but warms as it flows through the CAS in the tropics transporting 0.73, 0.71, and 0.56 PW of heat from the Pacific into the Caribbean for NARROW, WIDE, and WIDESHALLOW, respectively (Figure 4b). North Atlantic northward OHT decreases by 10.6–13.3% as heat is transported southward with an open CAS into the South Atlantic after warming in the tropics (Figure 4b); South Atlantic OHT reverses direction from 0.53 PW northward for

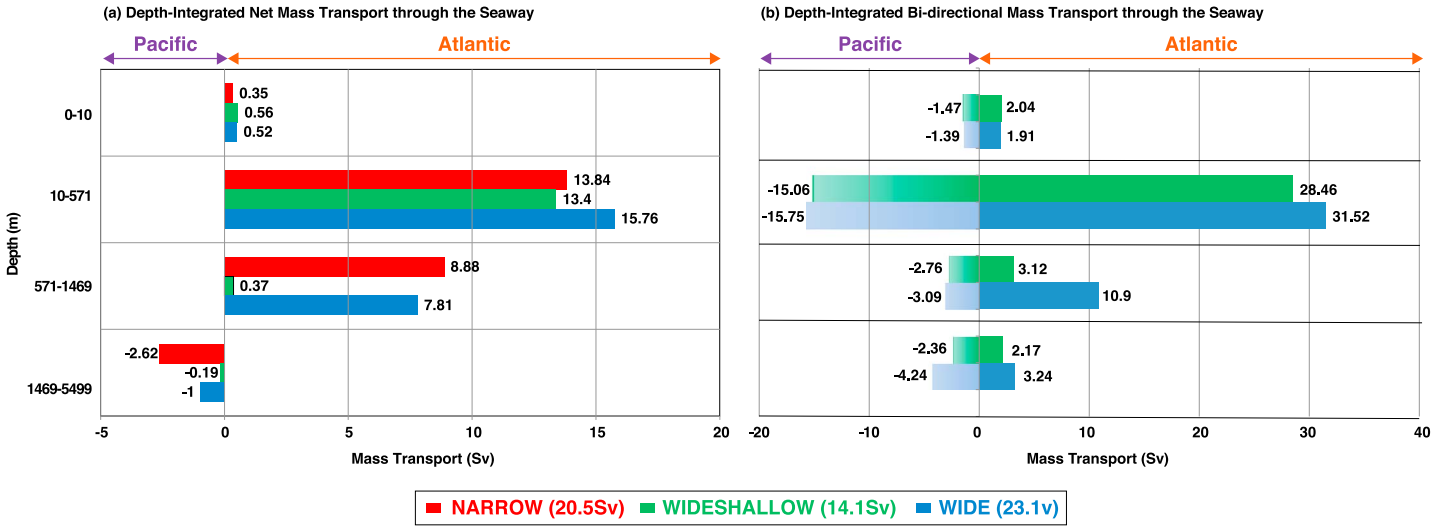

Figure 5. GFDL-ESM2G 100-year annual average depth-integrated (a) net interbasin (e.g., between the basins) and (b) bidirectional interbasin and intrabasin (e.g., within the basin defined within the transport box; Figures 1c and 1d) mass transport (Sv; 10^6 m^3/s) exchange in the Central American Seaway region computed along the yellow transect (Figure 1b; 77.5°W, 8.2°N) and within the boxes (Figures 1c and 1d; 18°–8°N; 100°–77°W) for NARROW and WIDE/WIDESHALLOW, respectively. Positive (negative) mass transport values indicate transport from the Pacific to the Caribbean (Caribbean to Pacific). Full depth-integrated net interbasin mass transport (Sv) values are included in the legend (parentheses). GFDL-ESM2G = Geophysical Fluid Dynamics Laboratory Earth System Model Version 2G.

CLOSED to 0.34, 0.36, and 0.15 PW southward for NARROW, WIDE, and WIDESHALLOW, respectively (Figure 4b). This OHT direction reversal with a CAS substantially warms the Southern Hemisphere (SH) ocean as the relatively warmer water in the South Atlantic increases OHT in the ACC (Figure 4b). Less heat (about half) is transported from the Pacific into the Indian Ocean through the ITF with an open CAS probably because mass transport is also decreased through the ITF, which transports less heat into the Indian Ocean (Figure 4b). The changes in water mass (Figure 4a) and salt transport (Figure 4c) represent a redistribution of mass and salinity with a CAS and are consistent with each other, while the changes in OHT (Figure 4b) with a CAS are nonlinear and are influenced by additional forcing factors, such as radiative processes, in response to changes in climate with a CAS.

The vertically integrated interbasin salt transport (Figure 4c) patterns are similar to the water mass (Figure 4a) and heat transport (Figure 4b) patterns with a CAS. Instead of transporting 719.7×10^6 kg/s of salt through the ITF in CLOSED, the water rerouted through the CAS also redistributes salinity by permitting salt transport into the Caribbean rather than through the ITF; 705.7×10^6, 795.3×10^6, and 486.2×10^6 kg/s increased CAS salt transport for NARROW, WIDE, and WIDESHALLOW, respectively (Figure 4c). This decreases salt transport in the Indian Ocean by ~58% (WIDESHALLOW) to 82% (NARROW and WIDE; Figure 4c). Salt transport into the Arctic Ocean via the Bering Strait and North Atlantic decreases ~36% to 55% and freshens the Arctic. Consistent with the primary mass transport pathway (Figure 4a), the primary salt transport pathway is through the CAS and into the South Atlantic; vertically integrated salt transports of 720.8×10^6, 805.3×10^6, and 499.5×10^6 kg/s, for NARROW, WIDE, and WIDESHALLOW, respectively (Figure 4c). Thus, water mass, salinity, and OHT increases in the South Atlantic because the CAS permits this transport compared to present day where the Central American isthmus blocks it.

With a CAS, annual, zonally integrated northward OHT decreases ~5% to 7% at 30°N and 8% to 21% at 30°S where the OHT reverses direction and becomes southward (Table 1). The annual, zonally integrated northward salt transport with a seaway are 2 to 8 times less at 30°N and 3 to 27 times less at 30°S (Table 1). While all stages of seaway shoaling result in decreases in zonally integrated northward OHT and salt transport (Figures S7a and S7b in the supporting information), they are largest in the SH and for WIDE and WIDESHALLOW (Table 1). WIDE has the largest difference in northward salt transport compared to CLOSED, especially in the SH, suggesting that earlier stages of closure may have had a larger impact on salt transport than later stages (Figure S7b in the supporting information). Two regions where the seaway increases northward salt transport are the Southern Ocean and the Northern Hemisphere (NH) extratropics (Figure S7b in the supporting information).

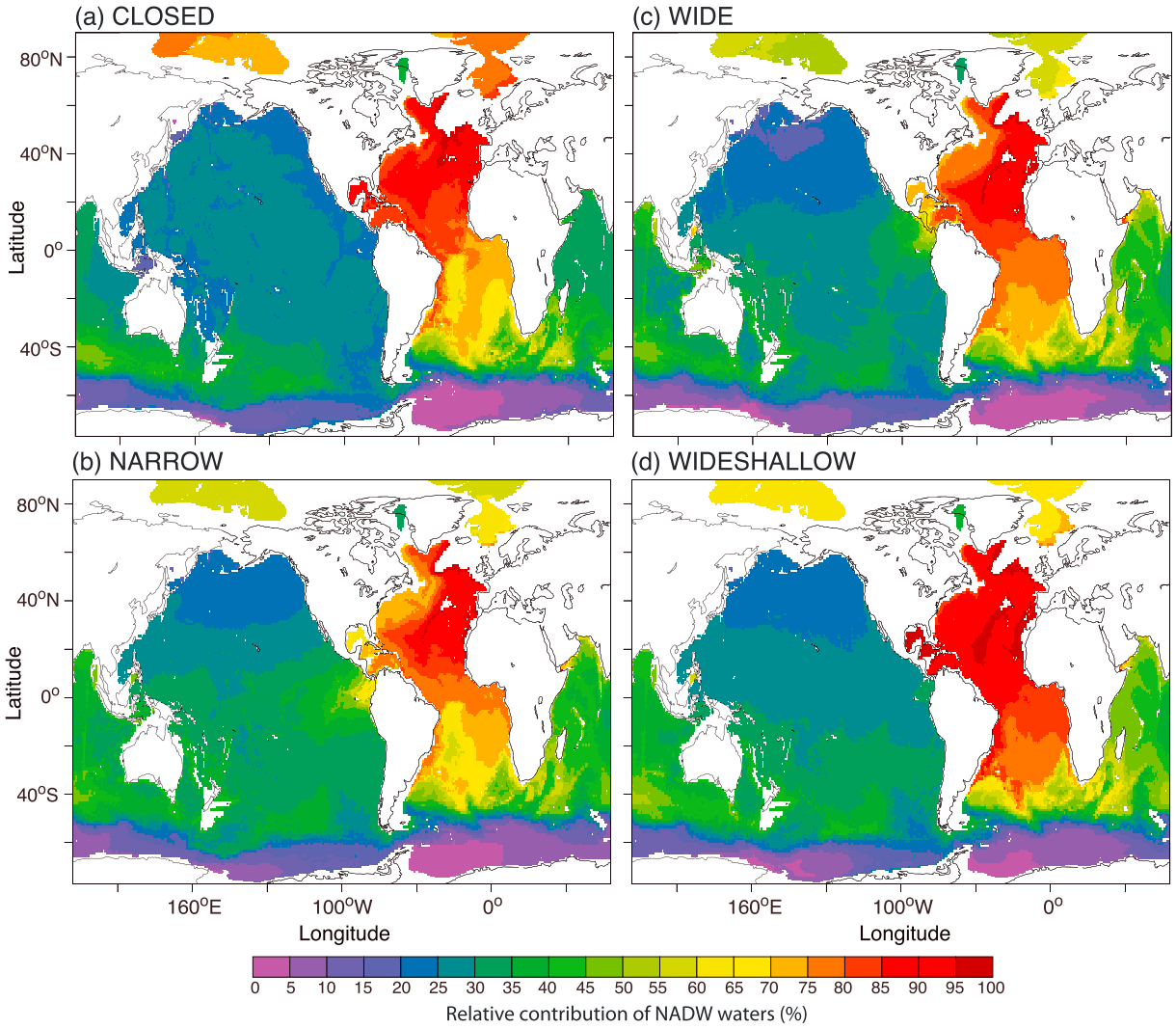

Figure 6. GFDL-ESM2G 100-year annual average relative contribution of NADW (%) characterized by salinity for (a) CLOSED, (b) NARROW, (c) WIDE, and (d) WIDESHALLOW based on Oppo and Fairbanks (1987) using end members to represent the average North Atlantic (20°–80°N; 30°–50°W) and Drake Passage (50°–70°S; 70°W) salinity from 1,469 to 5,499 m. GFDL-ESM2G = Geophysical Fluid Dynamics Laboratory Earth System Model Version 2G; NADW = North Atlantic Deep Water.

3.3. Seaway Impacts on Mean Climate

The changes in ocean heat and salt transport with an added seaway affect the global mean ocean state in several important ways, only some of which are sensitive to its topographic structure. Southward OHT with a seaway leads to a meridionally asymmetric annual average sea surface temperature (SST) response with a similar spatial pattern among all open CAS configurations (Figure 7; left). WIDE and WIDESHALLOW SSTs warm ~4 °C in the SH and cool ~3 °C in the NH compared to CLOSED; the spatial pattern is similar to NARROW but the magnitude of changes is slightly smaller (Figure 7; left). The bipolar SST response (Figure 7; left) is asymmetric with more SH warming than NH cooling resulting in global annual average SST warming of 0.32, 0.54, and 0.56 °C for NARROW, WIDESHALLOW, and WIDE, respectively (Table 1). The CAS has a strong local effect on SSTs in the CA region, cooling both sides of the seaway ~2 °C for all CAS configurations and decreasing the western Caribbean-Pacific SST gradient (Figure 7; left). There is anomalous warming (~1 °C) west of the CAS in the tropical central Pacific in WIDE and WIDESHALLOW. Overall, the CAS transports ocean heat southward along with water mass, warming the SH ocean consistent with OHT transport and is largest for WIDE and WIDESHALLOW.

The seaway redistributes global SSS similar to mass and salt transports and is largely independent of the CAS configuration (Figure 7; right). Local to the CAS, interbasin water mass transport and associated

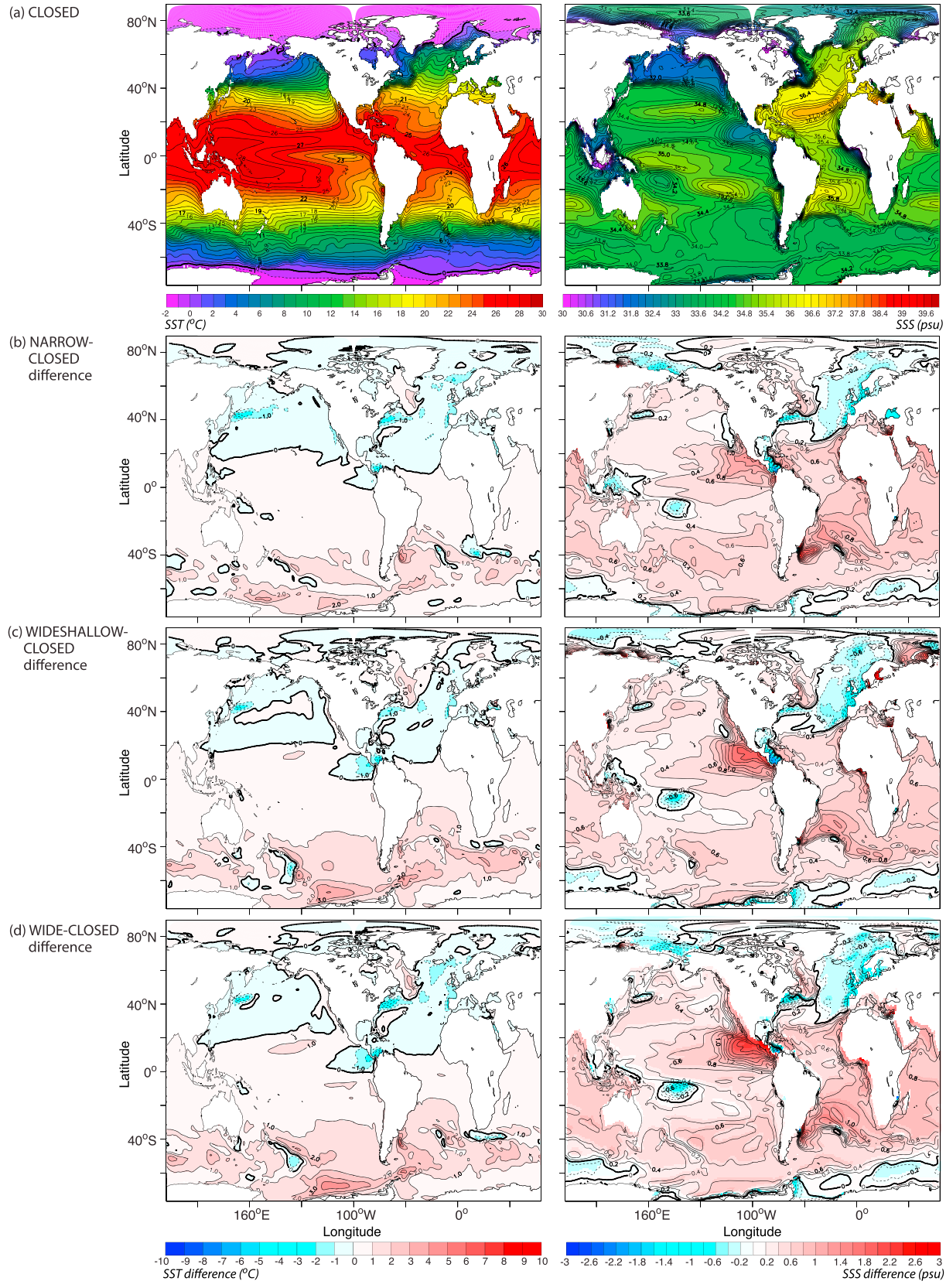

Figure 7. GFDL-ESM2G 100-year annual average (a) CLOSED, (b) NARROW-CLOSED, (c) WIDESHALLOW-CLOSED, and (d) WIDE-CLOSED differences in sea surface temperature (SST; °C; left) and sea surface salinity (SSS; psu; right). GFDL-ESM2G = Geophysical Fluid Dynamics Laboratory Earth System Model Version 2G.

salinity/freshwater fluxes from the influx of relatively fresh (salty) Pacific (Atlantic) water (section 3.2) and atmospheric hydrological response (Figure S8 in the supporting information) contribute ~2-psu surface freshening in the western Caribbean and ~3-psu surface salinification in the Eastern Pacific (Figure 7; right). These local changes decrease and reverse the direction of the western Caribbean-Pacific salinity gradient in this region (Figure 7; right). In general, the Atlantic and Pacific basins are saltier at the surface with a CAS, while the Arctic and North Atlantic high latitudes are fresher from reduced salt transport (Figure 7; right). SSS also decreases in the tropical West Pacific and North Atlantic, while the Labrador Sea—an area of deep water formation—is ~0.6 psu saltier with a CAS (Figure 7; right). Globally averaged, annual SSS is 0.43, 0.40, and 0.48 psu (or ~1%) higher for NARROW, WIDESHALLOW, and WIDE, respectively (Table 1). This suggests that the earlier stages of seaway shoaling (e.g., WIDESHALLOW) may have a larger impact on SSS and salt transport than the later stages (e.g., WIDE).

The large-scale changes in ocean heat and salinity with a CAS change the global upper (100 m) ocean density with similar spatial patterns among the open CAS configurations (Figure 8; left). Global annual average upper ocean density increases globally with a seaway; 0.25, 0.17, and 0.22 kg/m^3 for NARROW, WIDESHALLOW, and WIDE, respectively (Table 1), and are ~2 times larger than long-term centennial-scale variability. The spatial pattern of upper ocean density with a seaway (Figure 8; left) correlates more with changes in salinity (Figure 8; middle) than changes in temperature (Figure 8; right) on density. That is, the spatial pattern of changes in upper ocean density (Figure 8; left) is similar to the spatial pattern of changes in density from SSS (Figure 8; middle) with two exceptions; (1) surface cooling to the east of the seaway in the Caribbean (Figure 7; left) with upper ocean density increases (Figure 8; right) despite surface freshening (Figure 7; right), and (2) anomalous SST warming to the west of the seaway in the tropical central Pacific Ocean (Figure 8; left) with upper ocean density decreases (Figure 8; right) despite increased salinity (Figure 7; right). The overall offsetting density effects from salinity imply that the impact of a CAS on salinity is the main driver for changing upper ocean density, and the CAS changes the vertical structure of these properties also.

With the CAS, the annual average upper (100-m) ocean is denser in the Atlantic, Pacific, Southern, and Indian Ocean basins; below which it is less dense (Figure 9; left). There is an increase in upper ocean salinity in these basins (Figure 9; middle) and increased upper ocean density (Figure 9; left). Below 100 m, the Atlantic, Pacific, Southern, and Indian Oceans freshen (Figure 9; middle), contributing to reduced density (Figure 9; left) along with warming (Figure 9; right) that extends to the bottom of these basins. Therefore, while global annual average SSS increases (~0.5 psu) with a seaway (Table 1), below 100 m it freshens (Figure 9; middle) as the CAS redistributes ocean salinity horizontally and vertically over large spatial scales, consistent with the changes in global ocean circulation (section 3.2).

3.4. Seaway Impacts on Global Overturning Circulation

These changing water mass characteristics drive only moderate changes in circulation in our simulations (Figure 2). While the overall vertical and horizontal structure of the global MOC is similar with and without a CAS, there are noted differences. First, the northward extent of AABW in the Atlantic originating from the southern source region is suppressed with a seaway (Figures 2a–2d; left) due to SH warming partly from reduced sea ice extent freshening the Southern Ocean and reducing its density. AABW extends northward to ~42°N in CLOSED but the presence of a CAS suppresses this northern edge to ~20°N, north of which NADW depth increases by ~500 m at the expense of AABW for all open CAS configurations (Figures 6a–6d; right) consistent with the relative competition between the strength and extent of the AABW and NADW overturning cells (Cox, 1989; England, 1993). The maximum AMOC slightly deepens with all open CAS configurations (Figures 2a–2d; right) consistent with NADW deepening. Overall, there is slightly stronger overturning (Figures 2a–2d) and the changes in annual average maximum AMOC are similar among all open CAS configurations; ~2 Sv or 9% stronger with the deep seaways, and ~1 Sv or 4.5% stronger with the shallow sill seaway (Figure 2e), in contrast to other models.

While there are marginal changes to the structure of NADW, the CAS has a larger impact on the global redistribution of NADW properties, consistent with changes in global ocean circulation. At a given model grid box (x), the relative contribution of NADW to AABW at Drake Passage, representing a well-mixed water mass, characterized by salinity (S) was calculated by the equation of Oppo and Fairbanks (1987):

$$\%NADW = \left(\frac{S_x - S_{\mathrm{AABW}}}{S_{\mathrm{NADW}} - S_{\mathrm{AABW}}}\right) \times 100 \quad (1)$$

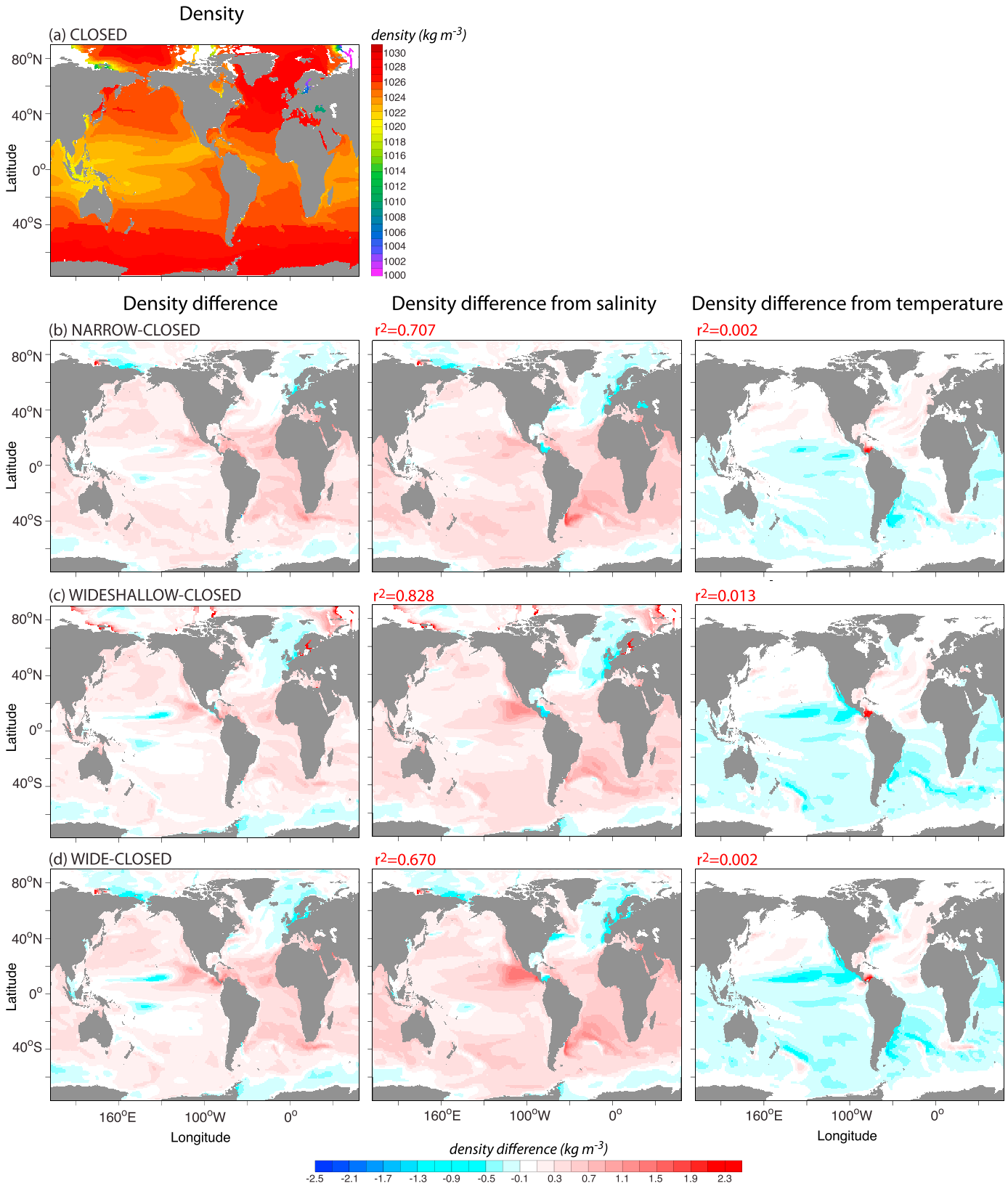

Figure 8. GFDL-ESM2G 100-year annual upper 100-m average (a) CLOSED, (b) NARROW-CLOSED, (c) WIDESHALLOW-CLOSED, and (d) WIDE-CLOSED differences in ocean density (kg/m^3; left), changes in density from only changes in salinity with a seaway (kg/m^3; middle), and from only changes in temperature with a seaway (kg/m^3; right). Coefficient of determination (r^2) values are shown in red. GFDL-ESM2G = Geophysical Fluid Dynamics Laboratory Earth System Model Version 2G.

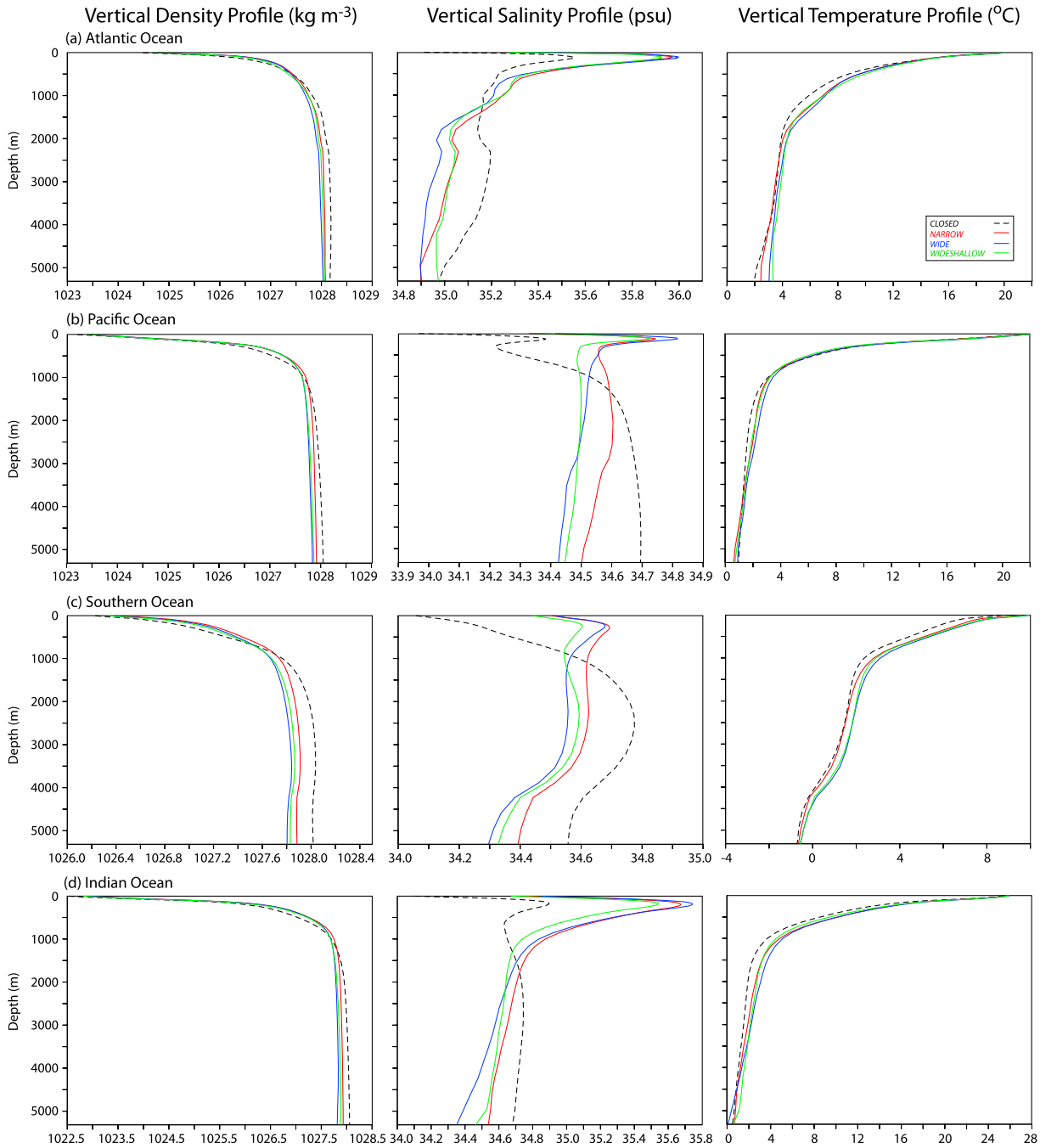

Figure 9. GFDL-ESM2G 100-year annual average vertical profiles of ocean density (kg/m^3; left), salinity (psu; middle), and temperature (°C; right) for the (a) Atlantic, (b) Pacific, (c) Southern, and (d) Indian Oceans for CLOSED (black dashed), NARROW (red), WIDE (blue), and WIDESHALLOW (green). GFDL-ESM2G = Geophysical Fluid Dynamics Laboratory Earth System Model Version 2.

where S_x is the average salinity from 1,469 to 5,499 m, S_{AABW} is the average salinity from 1,469 to 5,499 m at Drake Passage (70°W), and S_{NADW} is the average salinity from 1,469 to 5,499 m in the North Atlantic (20°–80°N; 30°–50°W). Overall, the Indian and South Pacific Oceans become more Atlantic like with respect to NADW salinity characteristics (i.e., increased salinity) with a seaway (Figure 6) as a result of the changing ocean circulation and salt transport (section 3.2). The general pattern is similar among the open CAS configurations, although there are regional differences. The deep seaways show the invasion of NADW into the Pacific through the CAS (Figures 6b and 6c) as indicated by increased relative contribution of NADW waters in the

EEP; from ~20% in CLOSED (Figure 6a) to ~60 (Figure 6c) and ~70% (Figure 6b) in WIDE and NARROW, respectively, representing higher salinity characteristics in the EEP with the deep seaways. There is an absence of NADW Pacific invasion (~30% relative contribution in the EEP) with the WIDESHALLOW sill depth (200 m) since it is above the level of NADW (Figure 6d). However, the overall spatial pattern of NADW relative contribution to AABW is similar globally among all open CAS configurations and suggests that there were large-scale, global changes in deep water with a CAS.

4. Summary of Results

The presence of the CAS, largely independent of the stage of shoaling, had a significant effect on the horizontal and vertical global ocean circulation by altering and redistributing water mass properties through changing interbasin transport throughout the depth of the ocean. The additional circulation pathways available with the seaway transported water mass and its characteristics through the CAS driven by SSH anomalies, rather than through the ITF, and continued in a global, zonal band throughout the SH. The water is warmed in the tropics after traveling through the seaway and flows into the South Atlantic. The increased southward OHT results in an asymmetric, bipolar SST response with global average warming dominated by the SH and extends throughout the depth of the ocean. The increased southward salt transport increases annual average global salinity from the surface to the upper 100 m and decreases global salinity below this level to the bottom. Upper 100-m global ocean density increases with a seaway and is directly attributed to changes in salinity, rather than changes in temperature, with the seaway. The seaway changes deep water circulation by suppressing the northward extent of AABW in the Atlantic and allowing AMOC to slightly strengthen (~2 Sv) and NADW to penetrate deeper in contrast to previous models, where the North Atlantic slightly cools in response to reduced northward OHT. The dispersion of Atlantic Ocean water mass characteristics in response to the global adjustment from the imposed forcing of the open CAS via the new circulation pathway changes the Indo-Pacific deep water circulation.

5. Discussion

Similar patterns among the various stages of seaway shoaling suggest that the evolution of the seaway did not have a large overall impact on the global ocean mean state and circulation until absolute closure. In fact, similarities in spatial patterns with the deep seaways imply that even a very small ~100-km-wide channel has a significant impact on global deep water circulation and a similar effect compared to a seaway about 20 times wider on long timescales (~1,000 years). Our results suggest that the circulation pathway established by the presence of the seaway in response to the SSH anomaly difference across the region, and not the particular seaway configuration, determines the changes in transport that drive changes in mean ocean state and deep water circulation. This mechanism by which the large-scale ocean adjusts in response to the imposed seaway forcing is similar to previous investigations of global ocean adjustments by other imposed forcings (Cessi et al., 2004; Cessi & Otheguy, 2003; Goodman, 2001; Hsieh & Bryan, 1996; Huang et al., 2000). Our results also have implications for comparing model and proxy data in constraining the stage of shoaling.

Our idealized experiment results are consistent with proxy data suggesting a decreased SST and SSS gradient between the Pacific and Caribbean when the seaway was present (Haug et al., 2001; Haug & Tiedemann, 1998; Keigwin, 1982; Maier-Reimer et al., 1990) and decreasing foraminiferal Mg/Ca ratios indicating a cooler Caribbean prior to ~4.4 Ma consistent with an influx of EEP water through an open CAS (Groeneveld et al., 2008). The model SST gradient calculated between ODP site 999 in the western Caribbean (Haug & Tiedemann, 1998) and ODP site 851 in the eastern Pacific (2°46′N, 110°34′W, water depth of 3,760 m; Cannariato & Ravelo, 1997) decreases from 2.28 °C without a seaway to 0.34, 0.92, and 1.17 °C for NARROW, WIDESHALLOW, and WIDE, respectively. The model SSS difference calculated between sites 999 and 851 also decreases, from 1.84 psu without a seaway to −0.28, −0.76, and −0.08 psu for NARROW, WIDESHALLOW, and WIDE, respectively. In particular, Haug et al. (2001) suggested that if due to salinity alone, the Pacific-Caribbean $\delta^{18}O$ gradient decrease of about 0.5‰ corresponds to a decrease of 1 psu with a seaway. Our model results at the same locations in the eastern Pacific and western Caribbean show that the early stage of shoaling (WIDE) has the largest decrease in Pacific-western Caribbean SSS gradient relative to the CLOSED case, although our results have a lower interbasin gradient decrease with a seaway. Furthermore,

our results of SH warming with an open CAS are consistent with recent Ross Sea and Antarctic proxy indicator reconstructions indicating reduced sea ice extent and duration before 3.3 Ma (McKay et al., 2012).

We also find a sharp Caribbean intrabasin gradient in SSS as a local response to the presence of the seaway; western Caribbean (ODP site 999) freshening and eastern Caribbean salinification. GFDL-ESM2G has a known bias where tropical Atlantic to Pacific moisture export is over-estimated in the model, resulting in a too salty/high SSS Atlantic bias relative to Pacific (Harrison et al., 2014). Therefore, our SSS gradient response with an open CAS (e.g., freshening in the western Caribbean) may be an underestimate given this relatively high Atlantic SSS bias. Our model results imply that the local seaway SSS response is not representative of the changes to the entire Caribbean or Atlantic basin SSS, and caution should be used when inferring Pacific-Caribbean SSS gradients and changes to the gradient with the seaway shoaling from proxy data obtained from the western Caribbean ODP sites. Perhaps at those sites, the proxy data capture the local seaway response (e.g., direct salinity/freshwater fluxes in the Caribbean with a CAS; section 3.3) and not changes to the entire basin. If this is true, then our understanding of the changes in global ocean mean state from changes in upper water exchange inferred from proxy data are not well known.

In contrast to previous model results that simulate transport through the seaway into the North Atlantic and weakening the AMOC, our model simulates seaway transport into the South Atlantic and a very small increase (~1–2 Sv) in the AMOC. Therefore, the mechanism by which our AMOC changes is through changing deep water circulation in the SH rather than changing buoyancy in the NH in response to altered upper-water exchange between the Pacific and Atlantic, or the "Panama Closure Hypothesis" (Haug & Tiedemann, 1998; Keigwin, 1982). The slightly nominal overturning with an open CAS, consistent with a stronger southward flow through the Atlantic, may be a result of a weaker and less layered ACC allowing the Atlantic to be more easily overturned. Our deep water circulation results are consistent with more recent benthic δ^{13}C proxy data obtained by additional South Atlantic ODP sites not previously available, showing significant and frequently stronger NADW with a CAS compared to present-day (Bell et al., 2015; Figure S2 in the supporting information), micropaleontological results suggesting reduced influence of southern component sourced water in the North Atlantic before 2.9 Ma (Ishman, 1996) and isotope proxy records (Raymo et al., 1990, 1992; Raymo, 1997; Woodruff & Savin, 1989) and sediment age mass distributions (Wold, 1994) both suggesting strong NADW formation during the Pliocene. This is in contrast to proxy data limited to the western Caribbean and deep equatorial Western Atlantic indicating reduced NADW with a CAS (Billups et al., 1998; Burton et al., 1997; Driscoll & Haug, 1998; Frenz et al., 2006; Haug et al., 2001; Haug & Tiedemann, 1998; Osborne et al., 2014; Steph et al., 2010), suggesting that previous, limited proxy data may not represent changes in the large-scale gradients and pathways in the Atlantic with a CAS because of bathymetric constraints from major ocean ridges, and/or differing water mass advection within the Deep Western Boundary Current and interior pathways. In addition, our model results of NADW penetration in the Pacific with the deeper CAS sills is consistent with results from Nisancioglu et al. (2003) suggesting relatively young NADW influence on deep sea Pacific sediment records during the Miocene.

There may be model-dependent factors that account for the differences between our results and previous models, such as model physics, horizontal grid discretization, numerics, and/or ocean horizontal and vertical spatial resolution. Yang et al. (2013) used a relatively coarse resolution version of our model with a different ocean formulation (CM2Mc) and simulated changes in transport through various global transects similar to our results. Conversely, with a seaway they found a 3.7-Sv weakening in the AMOC and no significant changes in deep ocean circulation structure except for a slightly smaller suppression of AABW northward extent than our findings. We speculate that differences between CM2Mc and GFDL-ESM2G, such as ocean grid horizontal resolution (3° in CM2Mc, 1° in GFDL-ESM2G) and different ocean physics, parameterizations, and ocean frameworks (Modular Ocean Model-based *z* coordinate in CM2Mc, GOLD-based isopycnal vertical coordinate in GFDL-ESM2G) may contribute to the different changes in AMOC between our results and Yang et al. (2013). Of these various mechanisms, GFDL-ESM2G tends to maintain the density of deep water when it is formed and, thus, has much deeper and more realistic AMOC than GFDL-ESM2M and CM2Mc (Dunne et al., 2012) allowing for more AMOC to penetrate below the 2,000-m sill depth.

This research highlights the need for additional model experiments with more complex and higher-resolution climate models, as well as additional/improved spatial resolution proxy data in the North Pacific, South Atlantic, and Southern Oceans, to better understand the mechanisms for changes in global deep

water circulation and its role on climate. While this manuscript isolates the role of the CAS on ocean circulation changes, other tectonic changes occurred around the time of the CAS shoaling. In particular, the reorganization of the Indonesian Gateway between 4 and 3 Ma changed the source waters feeding the ITF, leading to a subsurface freshening and cooling of about 4 °C and thermocline shoaling in the tropical Indian Ocean (Karas et al., 2009). They suggest that the tectonic changes to the Indonesian Archipelago possibly contributed to the present-day equatorial eastern Pacific cold tongue development, which has also been related to the gradual closing of the CAS (Chaisson & Ravelo, 2000; Steph et al., 2006). These and other such paleoreorganizations of ocean choke points could prove intriguing foci for future work akin to this study.

We plan on expanding this research by examining the mechanistic role of the seaway on the coupled physical climate mean state and variability (e.g., El Niño–Southern Oscillation, SH sea ice extent, NH glaciation implications) and changes in ocean biogeochemistry (e.g., ocean ventilation changes impacting carbonate sedimentation and preservation patterns) and atmospheric carbon implications. This research implies that small-scale, local perturbations have far-reaching effects on deep ocean circulation and is important for understanding global connections associated with possible future analogs, such as ice sheet collapse and freshwater input in response to climate change. As such, improving our mechanistic understanding of the interactions and feedbacks between ocean mean state and deep water circulation in an idealized experimental framework may improve predictions of future climate change.

Acknowledgments
This research was supported by the NOAA Oceanic and Atmospheric Research Graduate Studies Program. Model data and scripts are available at ftp://data1.gfdl.noaa.gov/users/Lori.Sentman/CAS/GFDL-ESM2G/. James R. Miller, Andrew Wittenberg, and Zachary Naiman reviewed earlier versions of this manuscript and provided valuable insight, including personal communication with Eric Galbraith. Alistair Adcroft, Matthew J. Harrison, and Zhi Liang provided technical support. Catherine Raphael produced and enhanced many of the illustration figures.

References

Antonov, J. I., Locarnini, R. A., Boyer, T. P., Mishonov, A. V., & Garcia, H. E. (2006). World ocean atlas 2005, volume 2: Salinity. In *NOAA Atlas NESDIS* (Vol. 62, p. 182). Washington, DC: U.S. Government Printing Office.

Bell, D. B., Jung, S. J. A., Kroon, D., Hodell, D. A., Lourens, L. J., & Raymo, M. E. (2015). Atlantic deep-water response to the Early Pliocene shoaling of the Central American Seaway. *Scientific Reports*, *5*(1), 12,252. https://doi.org/10.1038/srep12252

Billups, K., Ravelo, A., & Zachos, J. C. (1998). Early Pliocene deep water circulation in the western equatorial Atlantic: Implications for high-latitude climate change. *Paleoceanography*, *13*(1), 84–95. https://doi.org/10.1029/97PA02995

Broecker, W. (1998). Paleocean circulation during the last deglaciation: A bipolar seesaw? *Paleoceanography*, *13*(2), 119–121. https://doi.org/10.1029/97PA03707

Bryan, F. (1986). High-latitude salinity effects and interhemispheric thermohaline circulations. *Nature*, *323*(6086), 301–304. https://doi.org/10.1038/323301a0

Burton, K. W., Ling, H.-F., & O'Nions, K. (1997). Closure of the Central American Isthmus and its effect on deep-water formation in the North Atlantic. *Nature*, *386*(6623), 382–385. https://doi.org/10.1038/386382a0

Butzin, M., Lohmann, G., & Bickert, T. (2011). Miocene Ocean circulation inferred from marine carbon cycle modeling combined with benthic isotope records. *Paleoceanography*, *26*, PA1203. https://doi.org/10.1029/2009PA001901

Cannariato, K. G., & Ravelo, A. C. (1997). Pliocene-Pleistocene evolution of the eastern Pacific surface water circulation and thermocline depth. *Paleoceanography*, *12*(6), 805–820. https://doi.org/10.1029/97PA02514

Cessi, P., Bryan, K., & Zhang, R. (2004). Global seiching of thermocline waters between the Atlantic and the Indian-Pacific Ocean Basins. *Geophysical Research Letters*, *31*, L04302. https://doi.org/10.1029/2003GL019091

Cessi, P., & Otheguy, P. (2003). Oceanic teleconnections: Remote response to decadal wind-forcing. *Journal of Physical Oceanography*, *33*(8), 1604–1617. https://doi.org/10.1175/2400.1

Chaisson, W., & Ravelo, A. C. (2000). Pliocene development of the east–west hydrographic gradient in the equatorial Pacific. *Paleoceanography*, *15*(5), 497–505. https://doi.org/10.1029/1999PA000442

Coates, A. G., Collins, L. S., Aubry, M. -P., & Berggren, W. A. (2004). The geology of the Darien, Panama, and the late Miocene-Pliocene collision of the Panama arc with northwestern South America. *Geological Society of America Bulletin*, *116*(11-12), 1327–1344. https://doi.org/10.1130/B25275.1

Coates, A. G., & Obando, J. A. (1996). The geologic evolution of the central American Isthmus. In J. B. C. Jackson, A. F. Budd, & A. G. Coates (Eds.), *Evolution and environment in tropical America* (pp. 21–56). Chicago: University Chicago Press.

Collins, L. S., Coates, A. G., Jackson, J. B. C., & Obando, J. A. (1995). Timing and rates of emergence of the Limón and Bocas del Toro basins: Caribbean effects of Cocos Ridge subduction? In P. Mann (Ed.), *Geologic and tectonic development of the Caribbean plate boundary in southern Central America*, *Geological Society of America Special Papers* (Vol. 295, pp. 263–289). https://doi.org/10.1130/SPE295-p263

Corrigan, J., Mann, P., & Ingle, J. C. Jr. (1990). Forearc response to subduction of the Cocos Ridge, Panama-Costa Rica. *Geological Society of America Bulletin*, *102*(5), 628–652. https://doi.org/10.1130/0016-7606(1990)102<0628:FRTSOT>2.3.CO;2

Cox, M. D. (1989). An idealized model of the world ocean. Part 1: The global-scale water masses. *Journal of Physical Oceanography*, *19*(11), 1730–1752. https://doi.org/10.1175/1520-0485(1989)019<1730:AIMOTW>2.0.CO;2

de Boer, J. Z., Drummond, M. S., Bordelon, M. J., Defant, M. J., Bellon, H., & Maury, R. C. (1995). Cenozoic magmatic phases of the Costa Rican island arc (Cordillera de Talamanca). In P. Mann (Ed.), *Geologic and tectonic development of the Caribbean plate boundary in Southern Central America*, *Geological Society of America Special Papers* (Vol. 295, pp. 35–55).

Delworth, T. L., Broccoli, A. J., Rosati, A., Stouffer, R. J., Balaji, V., Beesley, J. A., et al. (2006). GFDL's CM2 global coupled climate models. Part I: Formulation and simulation characteristics. *Journal of Climate*, *19*(5), 643–674. https://doi.org/10.1175/JCLI3629.1

Delworth, T. L., & Zeng, F. (2016). The impact of the North Atlantic oscillation on climate through its influence on the Atlantic meridional overturning circulation. *Journal of Climate*, *29*(3), 941–962. https://doi.org/10.1175/JCLI-D-15-0396.1

Driscoll, N. W., & Haug, G. H. (1998). A short circuit in thermohaline circulation: A cause for Northern Hemisphere glaciation? *Science*, *282*(5388), 436–438. https://doi.org/10.1126/science.282.5388.436

Dunne, J. P., John, J. G., Adcroft, A., Griffies, S. M., Hallberg, R., Shevliakova, E., et al. (2012). GFDL's ESM 2 global coupled climate-carbon Earth System Models. Part I: Physical formulation and baseline simulation characteristics. *Journal of Climate*, *25*(19), 6646–6665. https://doi.org/10.1175/JCLI-D-11-00560.1

Dunne, J. P., John, J. G., Shevliakova, E., Stouffer, R. J., Krasting, J. P., Malyshev, S., et al. (2013). GFDL's ESM 2 global coupled climate-carbon Earth System Models. Part II: Carbon system formulation and baseline simulation characteristics. *Journal of Climate*, *26*(7), 2247–2267. https://doi.org/10.1175/JCLI-D-12-00150.1

Duque-Caro, H. (1990). Neogene stratigraphy, palaeoceanography and palaeobiogeography in Northwest South America and the evolution of the Panama Seaway. *Palaeogeography Palaeoclimatology Palaeoecology*, *77*(3-4), 203–234. https://doi.org/10.1016/0031-0182(90)90178-A

England, M. (1993). Representing the global-scale water masses in ocean general circulation models. *Journal of Physical Oceanography*, *23*(7), 1523–1552. https://doi.org/10.1175/1520-0485(1993)023<1523:RTGSWM>2.0.CO;2

Fox-Kemper, B., Danabasoglu, G., Ferrari, R., Griffies, S. M., Hallberg, R. W., Holland, M., et al. (2011). Parameterization of mixed layer eddies. III: Implementation and impact in global ocean climate simulations. *Ocean Modelling*, *39*(1-2), 61–78. https://doi.org/10.1016/j.ocemod.2010.09.002

Frenz, M., Henrich, R., & Zychla, B. (2006). Carbonate preservation patterns at the Ceará Rise—Evidence for the Pliocene super conveyor. *Marine Geology*, *232*(3-4), 173–180. https://doi.org/10.1016/j.margeo.2006.07.006

Ganachaud, A., & Wunsch, C. (2003). Large-scale ocean heat and freshwater transports during the World Ocean Circulation Experiment. *Journal of Climate*, *16*(4), 696–705. https://doi.org/10.1175/1520-0442(2003)016<0696:LSOHAF>2.0.CO;2

Goodman, P. J. (2001). Thermohaline adjustment and advection in an OGCM. *Journal of Physical Oceanography*, *31*(6), 1477–1497. https://doi.org/10.1175/1520-0485(2001)031<1477:TAAAIA>2.0.CO;2

Groeneveld, J., Nurnberg, D., Steph, S., Tiedemann, R., Reichart, G. -J., Reuning, L., & Crudeli, D. (2008). The Pliocene Mg/Ca SST increase in the Caribbean: Western Atlantic Warm Pool formation, salinity influence or diagenetic overprint? *Geochemistry, Geophysics, Geosystems*, *9*, Q01P23. https://doi.org/10.1029/2006GC001564

Hallberg, R. (2000). Time integration of diapycnal diffusion and Richardson number–dependent mixing in isopycnal coordinate ocean models. *Monthly Weather Review*, *128*(5), 1402–1419. https://doi.org/10.1175/1520-0493(2000)128<1402:TIODDA>2.0.CO;2

Hallberg, R. (2003). The suitability of large-scale ocean models for adapting parameterizations of boundary mixing and a description of a refined bulk mixed layer model. Near-Boundary Processes and Their Parameterization: Proc. 'Aha Huliko'a Hawaiian Winter Workshop (pp. 187–203). Honolulu, HI: University of Hawaii at Manoa.

Harrison, M. J., Adcroft, A., & Hallberg, R. (2014). Atlantic watermass and circulation response to persistent freshwater forcing in two coupled general circulation models. *Climate Dynamics*, *42*(1–2), 59–68. https://doi.org/10.1007/s00382-013-1798-5

Harrison, M. J., & Hallberg, R. W. (2008). Pacific subtropical cell response to reduced equatorial dissipation. *Journal of Physical Oceanography*, *38*(9), 1894–1912. https://doi.org/10.1175/2008JPO3708.1

Haug, G. H., & Keigwin, L. D. (2004). How the Isthmus of Panama put ice in the Arctic. *Oceanus Magazine*, *42*(2). http://www.oceanusmag.whoi.edu

Haug, G. H., & Tiedemann, R. (1998). Effect of the formation of the Isthmus of Panama on Atlantic Ocean thermohaline circulation. *Nature*, *393*(6686), 673–676. https://doi.org/10.1038/31447

Haug, G. H., Tiedemann, R., Zahn, R., & Ravelo, A. C. (2001). Role of Panama uplift on oceanic freshwater balance. *Geology*, *29*(3), 207–210. https://doi.org/10.1130/0091-7613

Hsieh, W. W., & Bryan, K. (1996). Redistribution of sea level rise associated with enhanced greenhouse gas warming: A simple model study. *Climate Dynamics*, *12*(8), 535–544. https://doi.org/10.1007/BF00207937

Huang, R. X., Cane, M. A., Naik, N., & Goodman, P. (2000). Global adjustment of the thermocline in response to deepwater formation. *Geophysical Research Letters*, *27*(6), 759–762. https://doi.org/10.1029/1999GL002365

Ishman, S. E. (1996). A benthic foraminiferal record of middle to late Pliocene (3.15–2.85 Ma) deep water change in the North Atlantic. *Marine Micropaleontology*, *27*, 1656–1800.

Johns, W. E., Baringer, M. O., Beal, L. M., Cunningham, S. A., Kanzow, T., Bryden, H. L., et al. (2011). Continuous, array-based estimates of Atlantic Ocean heat transport at 26.5°N. *Journal of Climate*, *24*(10), 2429–2449. https://doi.org/10.1175/2010JCLI3997.1

Karas, C., Nürnberg, D., Gupta, A. K., Tiedemann, R., Mohan, K., & Bickert, T. (2009). Mid-Pliocene climate change amplified by a switch in Indonesian subsurface throughflow. *Nature Geoscience*, *2*(6), 434–438. https://doi.org/10.1038/ngeo520

Keigwin, L. D. (1982). Isotopic paleoceanography of the Caribbean and East Pacific: Role of Panama uplift in late Neogene time. *Science*, *217*(4557), 350–353. https://doi.org/10.1126/science.217.4557.350

Kirby, M. X., & MacFadden, B. (2005). Was southern Central America an archipelago or a peninsula in the middle Miocene? A test using land-mammal body size. *Palaeogeography, Palaeoclimatology, Palaeoecology*, *228*(3–4), 193–202. https://doi.org/10.1016/j.palaeo.2005.06.002

Kirtman, B., Power, S. B., Adedoyin, J. A., Boer, G. J., Bojariu, R., Camilloni, I., et al. (2013). Near-term climate change: Projections and predictability. In T. F. Stocker, et al. (Eds.), *Climate change 2013: The physical science basis. Contribution of Working Group I to the Fifth Assessment Report of the Intergovernmental Panel on Climate Change* (pp. 953–1028). Cambridge, United Kingdom and New York: Cambridge University Press. https://doi.org/10.1017/CBO9781107415324.023

Klocker, A., Prange, M., & Schulz, M. (2005). Testing the influence of the Central American Seaway on orbitally forced Northern Hemisphere glaciation. *Geophysical Research Letters*, *32*, L03703. https://doi.org/10.1029/2004GL021564

Krasting, J. P., Dunne, J. P., Stouffer, R. J., & Hallberg, R. (2016). Enhanced Atlantic sea-level rise relative to the Pacific under high carbon emission rates. *Nature Geoscience*, *9*(3), 210–214. https://doi.org/10.1038/ngeo2641

Locarnini, R. A., Mishonov, A. V., Antonov, J. I., Boyer, T. P., & Garcia, H. E. (2006). World Ocean Atlas 2005, Vol. 1: Temperature. In *NOAA Atlas NESDIS* (Vol. 61, p. 182). Washington, DC: U.S. Government Printing Office.

Lonsdale, P., & Klitgord, K. D. (1978). Structure and tectonic history of the eastern Panama Basin. *Geological Society of America Bulletin*, *89*(7), 981–999. https://doi.org/10.1130/0016-7606(1978)89<981:SATHOT>2.0.CO;2

Lunt, D. J., Valdes, P. J., Haywood, A., & Rutt, I. C. (2008). Closure of the Panama Seaway during the Pliocene: Implications for climate and Northern Hemisphere glaciation. *Climate Dynamics*, *30*(1), 1–18.

Maier-Reimer, E., Mikolajewicz, U., & Crowley, T. (1990). Ocean general circulation model sensitivity experiment with an open Central American Isthmus. *Paleoceanography*, *5*(3), 349–366. https://doi.org/10.1029/PA005i003p00349

Manabe, S., & Stouffer, R. J. (1988). Two stable equilibria of a coupled ocean-atmosphere model. *Journal of Climate*, *1*(9), 841–866. https://doi.org/10.1175/1520-0442(1988)001<0841:TSEOAC>2.0.CO;2

Marshall, L. G. (1985). Geochronology and land mammal biochronology of the transamerican faunal interchange. In F. G. Stehli & S. D. Webb (Eds.), *The great American biotic interchange* (pp. 49–85). New York: Springer. https://doi.org/10.1007/978-1-4684-9181-4_3

McKay, R., Naish, T., Carter, L., Riesselman, C., Dunbar, R., Sjunneskog, C., et al. (2012). Antarctic and Southern Ocean influences on Late Pliocene global cooling. *Proceedings of the National Academy of Sciences of the United States of America*, *109*(17), 6423–6428. https://doi.org/10.1073/pnas.1112248109

Mikolajewicz, U., & Crowley, T. (1997). Response of a coupled ocean/energy balance model to restricted flow through the Central American Isthmus. *Paleoceanography*, *12*(3), 429–441. https://doi.org/10.1029/96PA03542

Mikolajewicz, U., & Maier-Reimer, E. (1994). Mixed boundary conditions in ocean general circulation models and their influence on the stability of the models conveyor-belt. *Journal of Geophysical Research*, *99*(C11), 22,633–22,644. https://doi.org/10.1029/94JC01989

Mikolajewicz, U., Maier-Reimer, E., & Crowley, T. (1993). Effect of Drake Passage and Panamian gateways on the circulation of an ocean model. *Paleoceanography*, *8*(4), 409–426. https://doi.org/10.1029/93PA00893

Milly, P. C. D., Malyshev, S., Shevliakova, E., Dunne, K. A., Findell, K. L., Gleeson, T., et al. (2014). An enhanced model of land water and energy for global hydrologic and earth-system studies. *Journal of Hydrometeorology*, *15*(5), 1739–1761. https://doi.org/10.1175/JHM-D-13-0162.1

Molnar, P. (2008). Closing of the Central American Seaway and the Ice Age: A critical review. *Paleoceanography*, *23*, PA2201. https://doi.org/10.1029/2007PA001574

Montes, C., Bayona, G., Cardona, A., Buchs, D. M., Silva, C. A., Morón, S., et al. (2012). Arc-continent collision and orocline formation: Closing of the Central American Seaway. *Journal of Geophysical Research*, *117*, B04105. https://doi.org/10.1029/2011JB008959

Montes, C., Cardona, A., McFadden, R., Moron, S. E., Silva, C. A., Restrepo-Moreno, S., et al. (2012). Evidence for middle Eocene and younger land emergence in Central Panama: Implications for Isthmus closure. *Geological Society of America Bulletin*, *124*(5–6), 780–799. https://doi.org/10.1130/B30528.1

Murdock, T., Weaver, A., & Fanning, A. (1997). Paleoclimatic response of the closing of the Isthmus of Panama in a coupled ocean–atmosphere model. *Geophysical Research Letters*, *24*(3), 253–256. https://doi.org/10.1029/96GL03950

Nisancioglu, K. H., Raymo, M. E., & Stone, P. H. (2003). Reorganization of Miocene deep water circulation in response to the shoaling of the Central American Seaway. *Paleoceanography*, *18*(1), 1006. https://doi.org/10.1029/2002PA000767

Oppo, D. W., & Fairbanks, R. G. (1987). Variability in the deep and intermediate water circulation of the Atlantic Ocean during the past 25,000 years: Northern Hemisphere modulation of the Southern Ocean. *Earth and Planetary Science Letters*, *86*(1), 1–15. https://doi.org/10.1016/0012-821X(87)90183-X

Osborne, A. H., Newkirk, D. R., Groeneveld, J., Martin, E. E., Tiedemann, R., & Frank, M. (2014). The seawater neodymium and lead isotope record of the final stages of Central American Seaway closure. *Paleoceanography*, *29*, 715–729. https://doi.org/10.1002/2014PA002676

Rahmstorf, S. (1995). Bifurcations of the Atlantic thermohaline circulation in response to changes in the hydrological cycle. *Climate Change*, *378*, 145–149.

Rahmstorf, S. (2002). Ocean circulation and climate during the past 120,000 years. *Nature*, *419*(6903), 207–214. https://doi.org/10.1038/nature01090

Raymo, M. E. (1997). The timing of major climate terminations. *Paleoceanography*, *12*(4), 577–585. https://doi.org/10.1029/97PA01169

Raymo, M. E., Hodell, D., & Jansen, E. (1992). Response of deep ocean circulation to initiation of northern hemisphere glaciation (3–2 MA). *Paleoceanography*, *7*(5), 645–672. https://doi.org/10.1029/92PA01609

Raymo, M. E., Ruddiman, W. F., Shackleton, N. J., & Oppo, D. (1990). Evolution of Atlantic-Pacific d13C gradients over the last 2.5 m.y. *Earth and Planetary Science Letters*, *97*(3-4), 353–368. https://doi.org/10.1016/0012-821X(90)90051-X

Schiller, A., Mikolajewicz, U., & Voss, R. (1997). The stability of the North Atlantic thermohaline circulation in a coupled ocean-atmosphere general circulation model. *Climate Dynamics*, *13*(5), 325–347. https://doi.org/10.1007/s003820050169

Schneider, B., & Schmittner, A. (2006). Simulating the impact of the Panamanian seaway closure on ocean circulation, marine productivity and nutrient cycling. *Earth and Planetary Science Letters*, *246*, 367–380.

Sepulchre, P., Arsouze, T., Donnadieu, Y., Dutay, J.-C., Jaramillo, C., Le Bras, J., et al. (2014). Consequences of shoaling of the Central American Seaway determined from modeling Nd isotopes. *Paleoceanography*, *29*, 176–189. https://doi.org/10.1002/2013PA002501

Simmons, H. L., Jayne, S. R., St. Laurent, L. C., & Weaver, A. J. (2004). Tidally driven mixing in a numerical model of the ocean general circulation. *Ocean Modelling*, *6*, 245–263.

Steph, S., Tiedemann, R., Prange, M., Groeneveld, J., Nürnberg, D., Reuning, L., et al. (2006). Changes in Caribbean surface hydrography during the Pliocene shoaling of the Central American Seaway. *Paleoceanography*, *21*, PA4221. https://doi.org/10.1029/2004PA001092

Steph, S., Tiedemann, R., Prange, M., Groeneveld, J., Schulz, M., Timmermann, A., et al. (2010). Early Pliocene increase in thermohaline overturning: A precondition for the development of the modern equatorial Pacific cold tongue. *Paleoceanography*, *25*, PA2202. https://doi.org/10.1029/2008PA001645

Stocker, T. F. (1998). The seesaw effect. *Science*, *282*(5386), 61–62. https://doi.org/10.1126/science.282.5386.61

Stommel, H. (1961). Thermohaline convection with two stable regimes of flow. *Tellus*, *13*(2), 224–230. https://doi.org/10.1111/j.2153-3490.1961.tb00079.x

Sykes, L. R., McCann, W. R., & Kafka, A. L. (1982). Motion of Caribbean plate during last 7 million years and implications for earlier Cenozoic movements. *Journal of Geophysical Research*, *87*(B13), 10,656–10,676. https://doi.org/10.1029/JB087iB13p10656

Talley, L. D. (2003). Shallow, intermediate, and deep overturning components of the global heat budget. *Journal of Physical Oceanography*, *33*(3), 530–560. https://doi.org/10.1175/1520-0485(2003)033<0530:SIADOC>2.0.CO;2

Taylor, K. E., Stouffer, R. J., & Meehl, G. A. (2012). An overview of CMIP5 and the experiment design. *Bulletin of the American Meteorological Society*, *93*(4), 485–498. https://doi.org/10.1175/BAMS-D-11-00094.1

Thompson, L., Kelly, K. A., Darr, D., & Hallberg, R. (2003). Buoyancy and mixed-layer effects on the sea surface height response in an isopycnal model of the North Pacific. *Journal of Physical Oceanography*, *32*, 3657–3670.

Webb, S. D. (1985). Late Cenozoic of mammal dispersals between the Americas. In F. G. Stehli & S. D. Webb (Eds.), *The great American biotic interchange* (pp. 357–386). New York: Springer. https://doi.org/10.1007/978-1-4684-9181-4_14

Webb, S. D., & Rancy, A. (1996). Late Cenozoic evolution of the neotropical mammal fauna. In J. B. C. Jackson, A. F. Budd, & A. G. Coates (Eds.), *Evolution and environment in tropical America* (pp. 335–358). Chicago, Ill: University of Chicago Press.

Whitmore, F. C. Jr., & Stewart, R. H. (1965). Miocene mammals and Central American seaways. *Science*, *148*(3667), 180–185. https://doi.org/10.1126/science.148.3667.180

Wold, C. N. (1994). Cenozoic sediment accumulation on drifts in the northern North Atlantic. *Paleoceanography*, *9*(6), 917–941. https://doi.org/10.1029/94PA01438

Woodruff, F., & Savin, S. M. (1989). Miocene deep-water oceanography. *Paleoceanography*, *4*(1), 87–140. https://doi.org/10.1029/PA004i001p00087

Yang, S., Galbraith, E., & Palter, J. (2013). Coupled climate impacts of the Drake Passage and the Panama Seaway. *Climate Dynamics*, *43*(1-2), 37–52. https://doi.org/10.1007/s00382-013-1809-6

Yin, J., & Stouffer, R. J. (2007). Comparison of the stability of the Atlantic thermohaline circulation in two coupled atmosphere-ocean general circulation models. *Journal of Climate*, *20*(17), 4293–4315. https://doi.org/10.1175/JCLI4256.1

Zhang, X., Prange, M., Steph, S., Butzin, M., Krebs, U., Lunt, D. J., et al. (2012). Changes in equatorial Pacific thermocline depth in response to Panamanian seaway closure: Insights from a multi-model study. *Earth and Planetary Science Letters*, *317-318*, 76–84. https://doi.org/10.1016/j.epsl.2011.11.028